

MASTER THESIS

Thesis submitted in partial fulfillment of the requirements
for the degree of Master of Science in Engineering at the University of
Applied Sciences Technikum Wien
Degree Program Medical Engineering & eHealth

Modeling of flow and pressure characteristics in the model of the human upper respiratory tract under varying conditions

By: Bc. Adéla Karlíková
Student Number: 1910228025
Supervisor 1: Ing. Richard Paštěka MSc.
Supervisor 2: Mathias Forjan MSc. PhD.

Vienna, 18th May 2020



Declaration of Authenticity

“As author and creator of this work to hand, I confirm with my signature knowledge of the relevant copyright regulations governed by higher education acts (see Urheberrechtsgesetz/ Austrian copyright law as amended as well as the Statute on Studies Act Provisions / Examination Regulations of the UAS Technikum Wien as amended).

I hereby declare that I completed the present work independently and that any ideas, whether written by others or by myself, have been fully sourced and referenced. I am aware of any consequences I may face on the part of the degree program director if there should be evidence of missing autonomy and independence or evidence of any intent to fraudulently achieve a pass mark for this work (see Statute on Studies Act Provisions / Examination Regulations of the UAS Technikum Wien as amended).

I further declare that up to this date I have not published the work to hand nor have I presented it to another examination board in the same or similar form. I affirm that the version submitted matches the version in the upload tool.”

Place, Date

Signature

Kurzfassung

Ziel dieser Masterarbeit ist es, ein 3D-Modell der oberen Atemwege gemäß dem aus CT-Daten segmentierten Originalmodell erstzustellen, unterschiedliche Bedingungen auf den Luftstrom im Modell anzuwenden und anschließend die Änderung der Eigenschaften von Geschwindigkeit und Druck zu bewerten. Das Modell der oberen Atemwege wurde in der Schnittstelle der Computational Fluid Dynamics-Software ANSYS realisiert, und die Navier-Stokes-Gleichungen wurden zur Modellierung des Luftstroms innerhalb des Modells verwendet. Zunächst wurde ein einfaches 2D-Modell erstellt, um sich mit der ANSYS-Schnittstelle vertraut zu machen. Darüber hinaus wurde das 3D-Modell der oberen Atemwege konstruiert und Geschwindigkeits- und Druckeigenschaften unter verschiedenen Bedingungen modelliert. Diese Bedingungen umfassen die unterschiedliche Platzierung und Anzahl der Probenahmelücken innerhalb des Modells sowie die Auswahl verschiedener Kombinationen von Einlässen. Schließlich werden die Ergebnisse zusammen mit den Abbildungen der unter verschiedenen Bedingungen modellierten Modelle präsentiert und ausgewertet. Das 3D-Modell der oberen Atemwege bedeutet einen Kompromiss zwischen Rechenlast und Modellkomplexität und kann als Grundlage für weitere Forschung verwendet werden.

Schlagwörter: Modell der oberen Atemwege des Menschen, Navier-Stokes Gleichungen, CFD, Modellierungssoftware, ANSYS Fluent

Abstract

The aim of this master's thesis is to create 3D model of upper respiratory tract (URT) according to the original model segmented from CT data, apply different conditions to the air flow inside the model, and afterwards, evaluate the change of characteristics of velocity and pressure. The model of URT was realized in the interface of Computational Fluid Dynamics software ANSYS and the Navier-Stokes equations were used for modeling the air flow inside the model. Firstly, simple 2D model was created for familiarization with the ANSYS interface. Furthermore, the 3D model of URT was constructed, and velocity and pressure characteristics were modeled under varying conditions. These conditions include different placement and quantity of sampling gaps within the model and choice of different combinations of inlets. Finally, the results are presented and evaluated along with the illustrations of the models modeled under varying conditions. The 3D model of URT means a compromise between computational load and model complexity and can be used as a basis for further research.

Keywords: Human upper respiratory tract model, Navier-Stokes equations, CFD, modelling software, ANSYS Fluent

Acknowledgements

I would like to express my sincere gratitude to my supervisor Ing. Richard Paštěka, MSc. for his professional help, support and guidance during the entire term of creating my master's thesis and, also, for enabling me to write my thesis under his supervision.

I want to give, also, my thanks to Mathias Forjan, MSc. PhD. for his supervision over my master's thesis.

Special thanks go to Ing. Igor Fabian Tellez Ceja, who had an unbelievable patience with me while writing this thesis. Thank you so much for your great help, spent time and for your kindness. Thank you for helping me grow. In my career, in life, in love.

Greatest thanks belong to my mum, who supports me my whole life and who always believed that I can reach my dreams. Thank you for everything you do for me and thank you for being my mum. With all my love, this thesis is dedicated to you as an expression of my gratitude.

Table of Contents

1	Introduction	6
1.1	Motivation	6
1.2	Aims	6
1.3	Objectives.....	7
2	Anatomy and physiology.....	8
2.1.1	Nose and oral cavity	8
2.1.2	Pharynx.....	9
2.1.3	Larynx	9
2.1.4	Trachea and lower respiratory tract	10
2.1.5	Mechanics of breathing.....	12
3	Computational fluid dynamics.....	13
3.1	Physics of fluid.....	14
3.1.1	Viscosity	14
3.1.2	Density.....	15
3.1.3	Reynolds number	15
3.2	Navier-Stokes equations.....	16
3.2.1	Conservation Law	16
3.2.2	Continuity equation.....	16
3.2.3	Momentum equation.....	17
3.3	Spatial discretization	18
3.3.1	Finite volume method	19
4	Particle deposition	20
4.1	Aerosols.....	20
4.2	Mechanism of particle deposition.....	20
5	Methods and Materials.....	22
5.1	Principles of computational modeling	22
5.1.1	Pre-analysis – Fusion 360.....	22
5.1.2	ANSYS Workbench and ANSYS Fluent.....	22
5.1.3	Geometry.....	22
5.1.4	Generation of the mesh	23
5.1.5	Model Set up.....	24
5.1.6	Numerical solution – contours	24
5.1.7	Workflow of the analysis in ANSYS	25
5.1	Choice of parameters.....	26

6	Results.....	27
6.1	2D model of the cylindrical pipe.....	27
6.1.1	Geometry and meshing.....	27
6.1.2	Initial and boundary conditions, registration of the governing equation.....	27
6.1.3	Analysis and results.....	28
6.2	3D model of the laminar flow within the bend pipe.....	30
6.2.1	Geometry and meshing.....	30
6.2.2	Initial and boundary conditions	30
6.2.3	Analysis and results.....	30
6.3	Simplified 3D model of the fluid flow	32
6.3.1	Design of the model.....	32
6.3.2	The description of the individual model analyzes	34
6.3.3	Analysis of the placement of the sampling gap.....	40
6.3.4	Summary of results.....	49
6.4	Particle deposition	50
7	Discussion.....	52
8	Conclusion	54
	List of Figures	57
	List of Tables	59
	List of Abbreviations	60
	A: Figures of modelled characteristics of the air flow under varying conditions	61

1 Introduction

Computational fluid dynamics is a method, which had no much use in medicine for long years. Nowadays are these techniques more and more of a great interest in current respiratory research. To simplify and speed up the research of the medicaments for treating breathing problems, it is important to obtain trustworthy model of upper respiratory tract, its flow, pressure and velocity characteristics and also to determine the passage of the particle through the respiratory tract.

Human respiratory system is very complex and when the air is passing the lumen of airways, the direction of air can change in a moment, which can lead to unwanted secondary processes of the airflow. Hence, the experimental investigations can be deficient and can lead to very inaccurate results. For this reason, a multiple of CFD modelling software were developed to help the analysis of the fluid movement. The study of respiratory airflow dynamics can provide relevant information about how the air and small particles behave in the respiratory tract for enhancing inhalation therapy applications and diagnostics based on aerosol. [1], [2]

1.1 Motivation

In this master's thesis the task is to find a solution of how to create trustworthy URT air flow model and simulate the air flow under varying condition. Mathematical modeling is very effective method by means of which we can explore the properties of the examined object, even if the real object does not physically exist. Nowadays the mathematical models are realized using computers. By means of computer simulation we can experiment with the model without worrying about its destruction, as in the case of the real models, tune in its properties and significantly increase the development and save costs.

Also, there can be seen a big educating potential in this task, as a lot of students struggle to imagine, how the air really flows through each part of the upper respiratory tract. This thesis can help them to create the picture of how the air flows inside the URT under varying conditions, for example pressure and velocity characteristics, since in this thesis the flow approaching the real human URT air flow is created.

Secondly the motivation to focus on this topic is to develop basic URT model, which can further be used for simulation the conditions dealing with breathing problems. For example, URT model of the patient with asthma. This can lead to the analysis of how to enhance the diagnoses of the patients and possibly develop more effective treatment of asthma.

1.2 Aims

The aims of this master's thesis are to process the model of the URT in the CFD software, to show different characteristics of the velocity and pressure within the model under varying conditions, such as different placement and quantity of sampling gaps and choice of different combinations of inlets and to demonstrate how the basic rules of physics of fluids influence the behavior of the air within the model under varying conditions.

1.3 Objectives

In order to meet the aims, the model of the URT will be proceeded in the CFD modeling software ANSYS Workbench. After that, contours of the models under varying conditions will be shown and the changes of the flow will be described based on visual perspective. Finally, the analysis of the models will be performed using ANOVA and pair t-test in order to evaluate the changes of the flow characteristics, such as velocity and pressure.

2 Anatomy and physiology

For deeper understanding of the principle of this master's thesis, it is necessary to get familiar with the anatomy and physiology of the breathing system. This part provides better view especially on the upper respiratory part, because that is the subject of our research. Nevertheless, whole respiratory tract will be briefly described.

The respiratory system consists of nose, mouth, throat (pharynx), voice box (larynx), windpipe (trachea), large airways (bronchi) and lungs; and is divided into upper and lower respiratory tract. The upper respiratory tract (URT) includes nose, pharynx, larynx and trachea; the lower respiratory tract contains bronchi and lungs. [3]

Respiratory system provides the connection between external environment and capillary blood vessels. Due to this contact, every cell in the human body can receive renewed metabolic gases, such as oxygen (O₂), which they use for metabolic reactions to create an energy. At the same time, as a product of these reactions carbon dioxide (CO₂) is released. Then, it must be quickly removed from the body cells, as it produces acidity, which is toxic to the cells. If any of the processes fails in its function, it can lead to the disruption of the homeostasis and the body cells start to die very fast. [4]

2.1.1 Nose and oral cavity

The air enters and leaves the human body via nose or oral cavity. It is well known that the nose is a most effective organ in humidification and heating. The nose conserves heat and water by condensing expired air savings, and then use these to heat the air up to 32°C and moisturizes up to 90% relative humidity. [5]

Another very important function happening inside the nose cavity is filtering ambient air from particles, which try to enter into the respiratory system and can cause problems with obstruction or irritation inside the respiratory tract. Filtering happens with the help of mucosa, which is very sticky. [6]

The nose consists of external nose, that is the extension of the bone and cartilage and is covered by skin. Its entryways are so called nostrils, which lead air to nasal vestibules. Nasal vestibules then join together and create internal nose - big cavity, that further continues as an airway through the posterior nares into pharynx. Nasal cavity is also connected to paranasal sinuses, that are air-filled spaces inside the bones, that surround the nose (frontal, ethmoid, sphenoid and maxillary sinuses). These sinuses also help the air to get warmer and moister and amplify sound of the voice. [3], [4], [8]

The mouth is initially used for processes of eating, swallowing of the food pieces and articulating of the speech. However, the mouth can be involved in breathing, anytime there is an obstruction in the nose or during the exercise. The air from the mouth goes straight to the respiratory tract, so the function of filtering, warming and moisturizing is very limited. [3], [6], [9]

2.1.2 Pharynx

Pharynx, also called throat, is a tube 13 cm long, that starts at the internal nares and extends to the larynx. Its function is to swallow food and pass the air down into larynx. It has skeletal muscles on the walls, which helps to move the food down. Sometimes there can happen a situation, that the food swallowed by mouth tries to pass from pharynx into the larynx and therefore reach trachea and bronchi. The interruption of breathing or elevation of the larynx should help to prevent this problem. There are also some other protective reflexes to push food or liquid from lower airway as fast as possible, e.g. coughing and gag reflex.[4] [6]

Pharynx is divided into 3 portions: nasopharynx, oropharynx and laryngopharynx.

Nasopharynx is the superior portion of the whole pharynx. There are five openings in the walls of nasopharynx; 2 internal nares, 2 opening that lead to eustachian tubes and 1 opening to oropharynx. This part also contains pharyngeal tonsils, which protect the body from infection, because they catch viruses and bacteria on their surface. Nasopharynx also help to equalize air pressure between pharynx and middle ear. [4]

The *oropharynx* is located posterior to the mouth and the food and air passing through the mouth is lead into the oropharynx and further to laryngopharynx. This region is most critical in swallowing and also joins the oral cavity with nasopharynx. It has the openings called fauces, that is an opening at the end of the mouth into a throat. There is a small flap called valve, which consist of soft palate and uvula. This projection closes the nasopharynx off when eating to prevent food to go up to the nasopharynx. [8], [11]

The *laryngopharynx*, also named as hypopharynx, is located behind the larynx. The division of the oropharynx from the laryngopharynx is the tip of the epiglottis. At the inferior border of the cricoid cartilage the laryngopharynx changes into oesophagus. [8], [9], [10]

2.1.3 Larynx

Larynx, also called voicebox, is a short path, that connects laryngopharynx with trachea. The wall of the larynx is made out of 9 cartilages; there are 3 single cartilages (thyroid cartilage, epiglottis, cricoid cartilage) and 3 are in pairs (arythenoid, cuneiform and corniculate cartilages). Very important are arytenoid cartilages, because they help to form the voice of the person. [10]

Up to the point where the larynx starts, food and air shared the same path. From this spot the food goes to oesophagus and air into the larynx and further to trachea. To prevent the food to enter to trachea, larynx contains large, leaf-shaped piece of elastic cartilage called epiglottis covered with epithelium. When the process of swallowing begins, pharynx and larynx rise, and pharynx widen to receive food and liquids. Epiglottis causes the movement down and therefore, closes the entrance of larynx in order to protect unwanted particles (e.g. food, liquids, smoke, dust) to enter to the larynx and further to the lungs. If by mistake food enters the larynx, cough reflex occurs in order to expel the material from the respiratory tract. [4],[8]

The biggest cartilage of the larynx is thyroid cartilage, also called Adam's apple. It gives the triangular shape to the anterior wall and is characteristically bigger in men than in women. The upper respiratory tract is shown on the figure 1. [9]

The main function of larynx is respiration because it serves as an airway path. Its function occurs also in protecting the airways against the entrance of food and drink. Last but not least, the larynx functions as the organ of voice production (thence: voice box). [3]

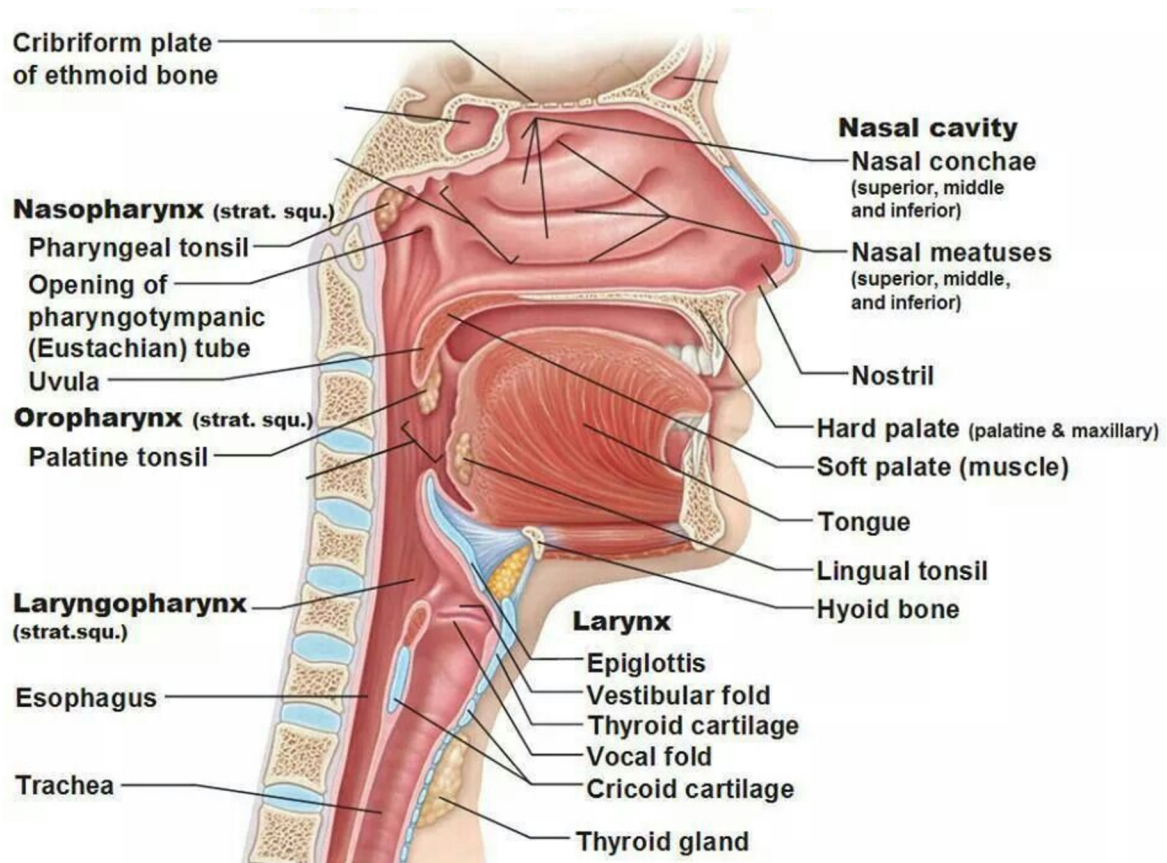


Figure 1: Anatomy of the upper respiratory tract [8]

2.1.4 Trachea and lower respiratory tract

Once the air passes through the larynx, it arrives into the trachea, which is also called windpipe. The trachea is attached to the larynx and lies anterior to the oesophagus. The epithelium of the trachea provides the same protection against dust as the epithelium of the nasal cavity. This serves as further control to prevent particles from coming into the lungs. There are special tools for reinforcing the trachea called cartilage rings to prevent the trachea from collapsing during inhalation. [4], [9]

The trachea splits into two mainstem bronchi (left and right bronchus) at its inferior ending. At this division point, there is a ridge named carina, which also helps to detect unwanted materials entering the trachea and stimulates the cough reflex. [8], [9]

Bronchi, Bronchial Tree, and Lungs

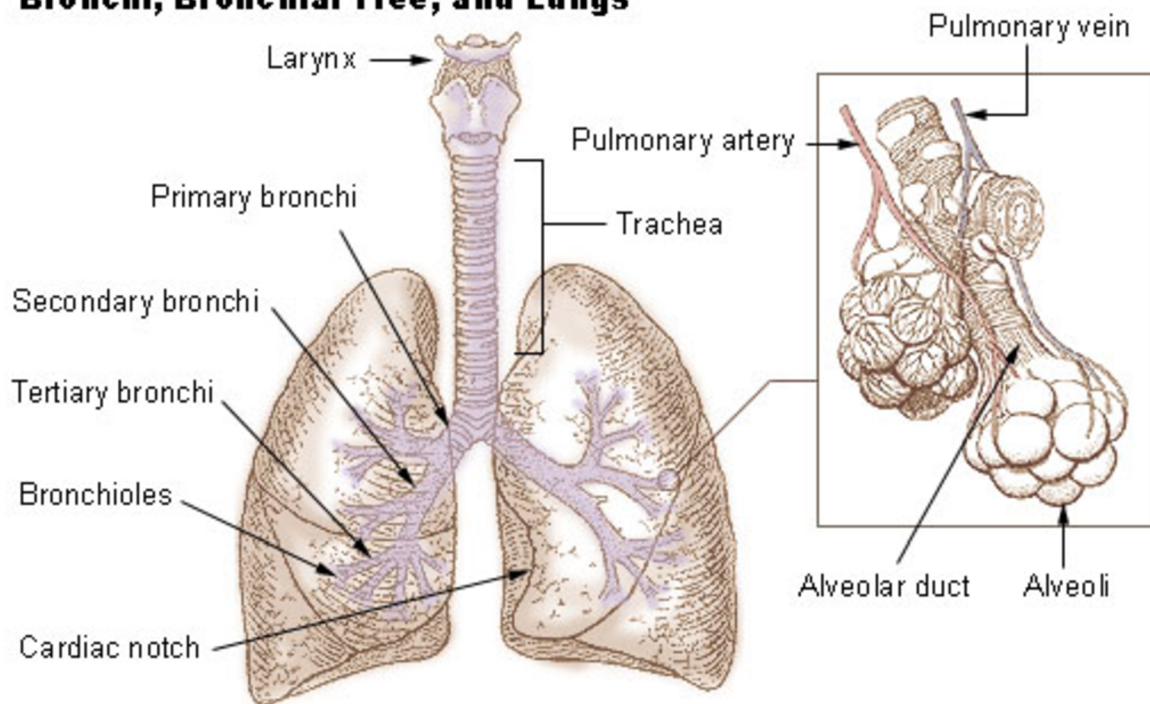


Figure 2: Anatomy of lower respiratory tract [8]

Main bronchi then split into smaller bronchioles. There occurs a lot of divisions, which is the reason why the lower respiration tract is called Tracheobronchial tree. At every division point (also called generation), the bronchioles branches into 2 or more smaller airways. In human body occurs in average 23 generations. First generations, closer to the trachea function as passageway of the air; further generations already participate in gas exchange. Not only trachea but also whole system of bronchi and bronchioles is supported with cartilage rings for prevention from collapse of the tubes. System of the lower respiratory tract can be seen on the figure 2. [3],[4]

Main organ for respiration is called the lungs. It is paired organ, which lie in the thoracic cavity, neighboring with the heart and other structures in mediastinum. Base of each lung touches the surface of the diaphragm. The lungs are not identical; the left lung has 2 lobes, because there has to be enough space for the heart, however the right lung has 3 lobes, separated by fissures. Because of this the right lung is obviously bigger and weights more than the left lung. In order the heart to fit, the left lung has indentation called the cardiac notch to accommodate the heart. [8], [9]

2.1.5 Mechanics of breathing

During respiration, which is the exchange of gases, occur 3 different stages; pulmonary ventilation, when air is exchanged between atmosphere and air space of the lungs, it consists of inhalation and exhalation; external respiration, when the exchange of the gases is made between the air spaces of the lungs and blood in pulmonary capillaries; internal respiration, when there is exchange of the gases between blood in systemic capillaries and tissue cells. In this thesis we will work just with the first gas exchange, the pulmonary ventilation. [4]

The way how the flow of the air moves between the atmosphere and lungs uses the same principle as when the blood flows through the body. The principle is pressure gradient. During inhalation, air goes into the lungs when the pressure inside the lungs is lower than the air pressure in the atmosphere and vice versa. This principle is based on the Boyle's Law, which says that in a closed space, pressure and volume are inversely related. This can be obtained by increasing the size of the lungs. [12]

Normal resting breathing is almost exclusively mediated by craniocaudal diaphragm movements. During inspiration, the diaphragm contracts, pulling lungs caudally, increasing its volume. Subsequently, the diaphragm relaxes, and the expiration is initiated. Resting breath is a passive process, as no muscle is involved. The only mechanism is the elastic forces of the lungs and of the thoracic wall, which due to the elastic properties of the tissues shrink to their original volume. This expels the same volume of air as it was inhaled – 500 ml. If there is a need to increase alveolar ventilation, as is the case during physical exercise, then the intercostal muscles also help. For keeping the airways of the lungs open, the pressure in the thoracic cavity needs to be always slightly negative. [4], [12]

3 Computational fluid dynamics

Computational Fluid Dynamics (CFD) is a branch of fluid dynamics, which provides a qualitative prediction of fluid flow with the help of mathematical modeling, numerical methods and software tools. For more complex problems the computers are used to provide the calculations required for simulation of the fluid flow. It is an effective tool how to visualize gas or liquid flow as well as to simulate how the gas or liquid affects the objects as it flows past. CFD software is based on Navier-Stokes equations, which describe the relation between the velocity, pressure, temperature and density of the moving fluid as described in chapter 3.1. [14], [31]

When we talk about study of fluid, we can examine the fluid flow problem in three ways: theory analysis, where the main aim is to find analytical solutions of governing equations or find the solution on the basis of theoretical arguments; experiment, where the researcher is using a model of the real object for examination; and simulation (CFD), where there are used computational procedures for finding the solution of the governing equations. [13]

CFD is still quite new method and is used more and more because of plenty of advantages it has in comparison with the methods of experiment. Let us take a look at the overview of the most important benefits of CFD. The great advantage concerns cost; experiments are often very expensive, as research community has to pay for all the equipment, for people providing the experiment and other expenses. Of course, CFD does not replace the physical measurement completely but the efficiency and overall cost can be significantly reduced. Another point concerns time effectiveness; experiments last a long time to finish, on the contrary, CFD can provide the results in few hours. Also, the CFD analysis is repeatable every time for every single problem, however, this cannot be said about all the experiments. Experiments can provide just limited amount of information, since the researchers focus on certain variables; CFD can display all the information possible of the result of the problem, also with higher resolution. Last but not least, safety is very important issue in conducting research, some experiments can be very difficult to provide, if not impossible; during CFD analysis this problem is negligible. [1], [13]

Of course, there can be also some arguments, that indicates, that CFD, too, has some disadvantages and is not 100% reliable. For instance, researcher working with CFD software can have a computer with limited computing power, which cause inaccuracy of the results. It may also happen, that the mathematical model of the problem can be chosen in the incorrect form and hence, the simulation is very limited. Last but not least, if the researcher does not have enough theoretical material and does not know exact values of input data, the model can include too much guessing and thus inaccuracies. The reliability of CFD is improved when talking about laminar and/or slow flows rather than turbulent and/or fast flows; about single-phase rather than multi-phase flows; about chemically inert flows rather than reactive flows. [1], [13]

3.1 Physics of fluid

Fluid is the common name for the liquids, gases and plasmas, whose common feature is fluidity. Fluidity means that liquids and gases are not able to maintain their constant shape due to easy relative motion of the particles; liquids deform easily when stressed and do not spring back to their original shape. They are also easy to divide. Fluids yield to shearing forces, whilst solids resist them. In this master's thesis the air is used as our fluid flow medium flowing from the mouth and nose to the trachea. [15]

3.1.1 Viscosity

Fluid resistance to shape change is called viscosity, which occurs only when the fluid is moving. Viscosity is a quantity that characterizes internal friction and depends primarily on the attraction forces between the particles. Liquids with higher attraction force have a higher viscosity. A higher viscosity also means greater hindering of the movement of the liquid or bodies in the liquid. [23], [24]

It is relevant to distinguish between kinematic ν and dynamic η viscosity. In Navier-Stokes equation calculations is used kinematic viscosity, however for example in Reynolds number formula the dynamic viscosity is used. The relation between them is:

$$\nu = \frac{\eta}{\rho} \quad (1)$$

where ρ is density, η is dynamic viscosity and ν is kinematic viscosity. [23]

When we talk about the real fluid, during fluid flow there exists inner friction which is defined by viscosity. The flowing fluid can be imagined as divided into many layers parallel to the direction of the flow. Individual layers can move towards each other with different velocity as shown on figure 3. The lowest velocity has the layer adjacent to the pipe wall. This layer will slower down the neighbor layer which is moving little faster than the outer layer. The highest velocity has the layer in the middle of the pipe. [23], [24]

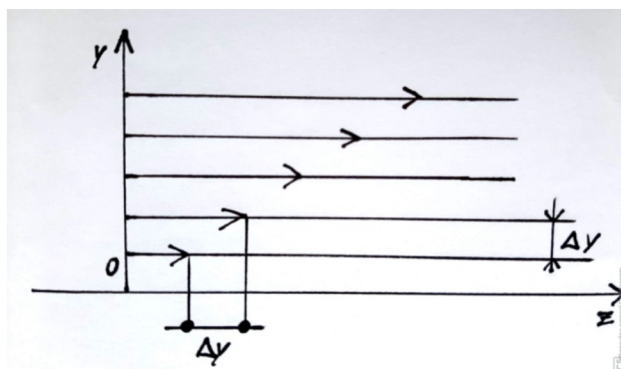


Figure 3: The partition of the velocities of the fluid depending on the distance from the pipe wall [24]

3.1.2 Density

Another very important feature of the fluid is density. Density is a physical quantity, which express the mass per unit volume of a substance. The density depends on temperature, pressure and mass. If the value of density during the whole experiment is constant, we are saying that the flow of such air is incompressible. [24]

Thanks to viscosity of the fluid and friction of the flowing fluid against the conduit walls is the velocity profile uneven. The velocity vector at any point of the fluid changes its size and direction over time. Despite of it, there is an effort to describe flow velocity, although, some turbulent flow can make it impossible. The distribution of velocity along the profile is not explored enough so far, so the mean cross-sectional velocity is used in many cases to describe the flow velocity. In the case of this master's thesis, we are introducing the input flow velocity as initial condition and thereafter, the simulation software tries to determine the flow velocity in every single point inside the URT separately. [23], [24]

3.1.3 Reynolds number

The Reynolds number is a dimensionless number characterizing the behavior of a flowing liquid. According to its value, it can be considered, whether the flow will be laminar or turbulent. This Reynolds number R_e value depends on the velocity of the flow v , the density of the fluid ρ , diameter of the pipe r and dynamic viscosity of the fluid η , see the equation:

$$R_e = \frac{v \cdot \rho \cdot r}{\eta} \quad (2)$$

Fluids transform from laminar flow to turbulent after exceeding the threshold value of the Reynolds number. For air is the threshold approximately 2320. If $R_e < 2320$, then the flow is laminar, which means that the velocity distribution is parabolic, as seen on the figure 4. [18]

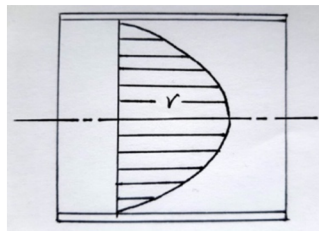


Figure 4: Velocity distribution in laminar flow of the fluid [18]

If $R_e > 2320$, then the flow is turbulent, vortices are created inside the pipe and the liquid is mixed. The velocity distribution is not parabolic as in laminar flow, see figure 5. [18]

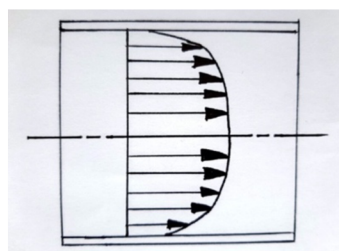


Figure 5: Velocity distribution in laminar flow of the fluid [18]

3.2 Navier-Stokes equations

Navier-Stokes equations are equations mathematically describing incompressible Newtonian fluid. The equations were derived by French Claude Louis Marie Henri Navier in 1827 and Irish George Gabriel Stokes in 1845, who derived it independently on each other. Mathematical analysis and numerical approximation of Navier-Stokes equations is very complicated process and until now the mathematical problem is still not completely solved. It can be analytically solved just in very few cases of simple flows; complex cases need to be solved numerically. [1]

3.2.1 Conservation Law

Navier-Stokes equations are the governing equations of Computational fluid dynamics, which are based on the conservation law of physical properties of fluid. The principle of conservation law is the change of properties, for example mass, energy, momentum; in an object it is given by input and output. For example, the change of mass in the object is defined as the difference between the mass entering into the system and mass exiting the system. If the difference of mass is equal to zero, then it means that the mass is constant. This is the proof of the conservation of the mass. [24]

The governing equations are based on the fundamental laws of fluid flow. The first is conservation of mass; the second fundamental law is conservation of momentum; and then there is conservation of energy, which is based on the first law of thermodynamics. In this thesis it is assumed that the density is constant, hence the flow can be called incompressible and, in that case, the energy equation does not need to be considered. [24]

3.2.2 Continuity equation

Continuity equation is simply a mathematical expression of the conservation of mass. It is assumed that density is constant, because there is the fact that the fluid in this master's thesis is incompressible; mass has to be also constant, because there is a requirement to reach mass conservation; and volume cannot change because of the applied formula herein

$$m = \rho \cdot V \quad (3)$$

The continuity equation says that the rate at which the mass enters into the system is equal to the rate at which the mass leaves the system plus the accumulation of the mass within the system. The continuity equation for the flow of the fluid with density ρ , velocity v and fluid velocity vector \mathbf{v} may be written as

$$\frac{\partial \rho}{\partial t} + \nabla \cdot (\rho \mathbf{v}) = 0 \quad (4)$$

In the case of an incompressible fluid, density is constant, which is, also, the case in this master's thesis, the continuity equation reduces to the following condition [17]

$$\nabla \cdot \mathbf{v} = 0 \quad (5)$$

3.2.3 Momentum equation

In order to derive the momentum equation to get the differential form of the equation, Newton's second law of motion has to be applied, see

$$F = m \cdot a \quad (6)$$

and, also, the pressure and viscous forces on the fluid particle and acceleration of the fluid particle has to be considered. In order to present the momentum equation, pressure forces, viscous forces and acceleration has to be introduced. [20]

Pressure forces

To see how to write the pressure term in Newton's second law of motion $F = m \cdot a$, the net pressure force per unit volume in x direction is described

$$F_{px} = -\frac{\partial p}{\partial x} \Delta x \Delta y \quad (7)$$

and, also, net pressure force in y direction is described

$$F_{py} = -\left(\frac{\partial p}{\partial x} i + \frac{\partial p}{\partial y} j\right) = -\nabla p \quad (8)$$

where F_{px} and F_{py} are net pressure volumes in x and y direction and p is pressure. [20]

Viscous forces

The viscous force is the force between the body and a fluid. The force acts on the body in the direction in which the fluid is moving relative to the body. Here it can be seen that the net viscous force τ in the x direction is

$$F_v = \frac{\partial \tau_{xx}}{\partial x} + \frac{\partial \tau_{xy}}{\partial y} \quad (9)$$

where τ_{xx} and τ_{xy} are the shear forces in x and y direction.

The same expression for the y direction can be written as well in the same manner (not shown). Then, when the equations of viscous force in x and in y direction are joined together, we will get the net viscous force per unit volume

$$F_{v/vol} = \mu \cdot \nabla^2 \cdot \mathbf{V} \quad (10)$$

where μ is a constant dynamic viscosity of the air, ∇^2 is Laplacian operator, \mathbf{V} is vector of volume. [20]

Acceleration

To complete the study of momentum equation, we have to understand the acceleration of the infinitesimal fluid particle in Eulerian frame of reference. The acceleration not only depends on the rate of change of velocity in x direction, but it also depends on how much the particle of the fluid within the pipe moves in the x direction, which is given by its velocity. Here we can see the acceleration in the x direction on and similarly we can make the acceleration equation in the y direction (not shown).

$$a_x = u \frac{\partial u}{\partial x} + v \frac{\partial u}{\partial y} \quad (11)$$

where u and v are velocities in the x and y directions. [20]

Differential form of Momentum equation

It is assumed that the flow is steady and that the density is constant, which means that the fluid is incompressible and, also, the fluid is Newtonian. So, when joining all parts together, the differential form of the Momentum equation can be determined

$$\rho(\mathbf{v} \cdot \nabla \mathbf{v}) = -\nabla p + \nu \nabla^2 \mathbf{v} \quad (12)$$

where \mathbf{v} is the fluid velocity vector, p is the fluid pressure, ρ is the fluid density, ν is the kinematic viscosity, and ∇^2 is the Laplacian operator. Each part of the equation corresponds to different forces:

$\rho(\mathbf{v} \cdot \nabla \mathbf{v})$ inertial forces,
$-\nabla p$ pressure forces,
$\nu \nabla^2 \mathbf{v}$ viscous forces. [17]

3.3 Spatial discretization

The computational model is a representation of physiological reality, which is expressed in the form of mathematical equations. Many processes and phenomena are described by differential equations. Model equations can be solved analytically or numerically. Analytical models provide accurate solution of the equations continuous in space and time and are therefore suitable for geometrically simple areas. The disadvantage of the analytical solution is the considerable theoretical and technical complexity and therefore the fact that it cannot always be used. There is a very wide class of equations that cannot be solved analytically. At that moment, other numerical methods are used. In order to solve more complicated problems and more complex geometries, it is advisable to use numerical models which, with a finite number of steps, find an approximate solution to the given equations. The basic types of numerical modeling methods include the finite difference method (FDM), finite element method (FEM) and finite volume method (FVM). Below the Finite volume method is described since this method is used in the modeling software ANSYS. [15]

3.3.1 Finite volume method

Finite volume method (FVM) is a discretization method for representing and evaluating partial differential equations expressing the conservation, balance or other quantities. The flow domain is divided into a number of small control volumes. The points, where the variables are stored, are typically defined at the center of each control volume. The control volume is the name for individual elements of the mesh. There can be also added extra boundary nodes, as it is shown on the figure 6. [21], [30]

Afterwards, the differential form of the governing equations over each control volume is integrated. Then, the interpolation function is applied to describe the variation of the given variable between the centers of each control volume. In this way, the discretization equation, how the resulting equation is called, formulates the conservation principle for the variable within the control volume. [21]

This method is based on applying the conservation principles over each small control volume and then the essential idea is to approximate the integral conservation law on each of the control volumes. This method is widely used in computational fluid dynamics, since this method is well suited for the numerical simulations of various types of conservation laws. [13], [16]

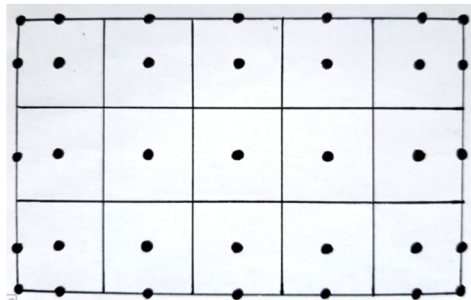


Figure 6: Division of the flow domain with extra nodes added [13]

Interpolation function

When formulating the behavior of elements between nodes, it is necessary to approximate solutions using predetermined simple functions. Polynomial interpolation functions are most often used. Advantages include easy integration or derivation of such a function. It is also possible to refine the solution by increasing the degree of polynomial. Higher-order elements contain, in addition to nodal points, other nodes that are located at the boundary or inside the elements because of the formulation using higher degrees of the polynomial. By increasing the order of the polynomial, it is possible to obtain a more accurate solution at the expense of increasing computational time. [6]

Equation (13) describes the example of the calculation of the c value outside the nodal point and it is therefore necessary to use the interpolation functions N_1 , N_2 and N_3 .

$$c(x, y) = N_1(x, y)c_1 + N_2(x, y)c_2 + N_3(x, y)c_3 \quad (13)$$

4 Particle deposition

Breathing is vitally important function and during everyday life, people not only inhale the air, but also small particles of aerosols. These particles can be very diverse, from tobacco smoke, through ashes and dust to water aerosols. It can happen that after inhaling the unhealthy aerosol particles for some amount of time, some respiratory disease may develop. In order to cure respiratory disease, for example the most common chronic disease nowadays – asthma, the medicament in the form of aerosol has to be provided. This is an example, that one type of aerosol can harm the respiratory tract and another type can heal it.

4.1 Aerosols

Aerosols are heterogeneous mixtures of a gas with small solid (smoke) or liquid (fog) particles or both. The dispersed particles have a size of 10 nm to 10 μm . The term particle itself then refers to a small individual object that can be chemically homogeneous (have the same chemical composition) or heterogeneous. The aerosol can be monodisperse, i.e. composed of particles of a small size range, or polydisperse.

The basic parameter that influences the behavior of a particle is its size. The size of a spherical particle is clearly defined by its diameter. For particles of a more complex shape, dimensional characterization is more difficult. Therefore, the concept of equivalent diameter is used, which is the diameter of a spherical particle for which the value of a certain physical quantity is identical with the observed particle.

For aerosols larger than 0.5 μm in the respiratory system, an aerodynamic equivalent diameter (abbreviated to aerodynamic diameter) is used, which means the diameter of a spherical particle with a density of 1000 kg/m^3 , which has the same sedimentation velocity in the gravitational field as the monitored particle.

4.2 Mechanism of particle deposition

The biggest influence on the depositing particles has the characteristics of the particles, such as the size, shape, electrical charge, or water solubility, further the anatomy of the respiratory tract and finally the way of breathing, such as the depth of breathing, the frequency, the breathing through the mouth or nose.

Deposition is the process where the particles are deposited on the surface of the respiratory tract. Mostly effective is the deposition for very small or very large diameters of particles. There are 4 ways of the particle deposition when coming through the respiratory tract – interception, impaction, sedimentation and diffusion, as shown on the figure 7.

Interception occurs, when the particle is moving very near the surface of the airway, so the particle touches the surface. Then it gets captured on the surface and stay there. Logically, the particle interception becomes more probable, when the airway diameter becomes smaller.

Impaction happens, when the particles do not follow the streamline and hits the opposite wall. Especially it occurs in the place of the bend in the respiratory system, because a lot of particles do not follow the original flow and have a tendency to travel along the original

flow. The possibility of impaction depends a lot on the velocity of the air and the particle mass. Since in nasopharyngeal region is very high speed of air and the URT is provided with a lot of bends, this mechanism appears here the most. If the particle is larger than $10\ \mu\text{m}$, then they are impacted right in the nose or mouth and do not continue any further.

Sedimentation is a phenomenon caused by gravity. As the particles pass through the air, the gravitational forces and air resistance overcome their buoyancy and it results in settling the particles on the surface of the lung. It is happening especially in the bronchi and bronchioles since there is the air velocity relatively low. Particles smaller than $0,5\ \mu\text{m}$ in diameter are not very influenced by this factor, on the other hand, increasing particle size really increases the chance of particles to deposit this way, especially the particles with diameter between $0,003$ and $5\ \mu\text{m}$ are deposited here. Other factors which can increase the deposition is the increasing particle density or length of time spent in the airways.

Diffusion also known as Brownian motion is a random motion of particles. Therefore, the particles deposit on the lungs wall mostly by coincidence. Smaller particles move more vigorously. This deposition mechanism is the most important in the small airways and alveoli, but very small particles can also be trapped in the upper respiratory tract.

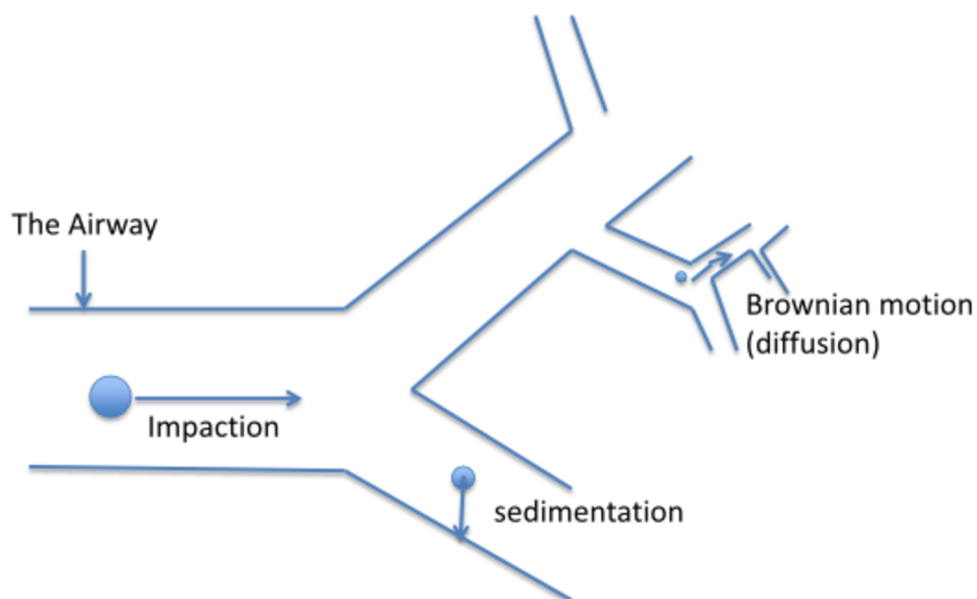


Figure 7: Illustration of different mechanisms of particle deposition [26]

All the information from the chapter 4 are referenced by these sources [26], [27], [28], [29].

5 Methods and Materials

5.1 Principles of computational modeling

Model is representation of reality and is always less detailed than the represented system however it can give us very good insight into the progress of the fluid flow in the examined model. In this chapter, the workflow of the modeling software ANSYS Fluent Workbench will be described. The individual interfaces of ANSYS will be described herein.

5.1.1 Pre-analysis – Fusion 360

The models with simple geometry, which are mostly created in SpaceClaim or DesignModeler, are not necessarily adjusted with another software tool. However, more complex geometries, which are mostly received from CT or other medical modalities, can contain some irregularities and errors. It is possible to reduce or even remove all the errors with the help of other tools than ANSYS. In this master's thesis, Fusion 360 from Autodesk was used as a model editing tool.

Fusion 360 is a modern 3D software tool, by which the models can be adjusted or transformed into another data type and then exported, so they can be used further in ANSYS. The main functions for this master's thesis in Fusion 360 are modifying functions, for example Reduce Facets, Remesh, Smooth, Plane Cut, Merge or Stitch. Very important function is Mesh to BRep, which change the STL file received from CT, into solid body, so the user can work with this model in ANSYS.

5.1.2 ANSYS Workbench and ANSYS Fluent

ANSYS Workbench is a platform, which provide complex and integrated simulation system. This platform ties together whole simulation process, the user is guided through the entire analysis and can select the modules and capabilities required for each simulation task.

ANSYS Workbench fluid analysis tools include two widely used softwares - ANSYS Fluent and ANSYS CFX. For the analysis in this master's thesis ANSYS Fluent was chosen, therefore, the main focus in this chapter will be on this software. ANSYS Fluent is one of the most popular commercial CFD software packages. It is based on the Finite Volume method, which is described in the chapter 3.3.1. This software contains wide modeling capabilities needed to model flow, turbulence, heat and so on. [22]

5.1.3 Geometry

Geometry is very useful part of the analysis. Easier geometries can be done in the Geometry interface, which consists of 2 possibilities – ANSYS SpaceClaim and ANSYS DesignModeler. ANSYS DesignModeler is a tool for the work with geometry which will be further used in CFD analysis. This software is more convenient for beginners since the interface is more intuitive for the user.

ANSYS SpaceClaim is by its function very similar with ANSYS DesignModeler, however, it was designed for more complex geometries. There is a lot of options for the work with geometry and the handling is easier. It is very fast and intuitive 3D modeling software which can prepare the model for the simulation, even if model was originally created in different software.

For designed or adjusted models in Fusion 360, it is still necessary to process the model in the Geometry interface, where the whole geometry is checked, whether there are some errors, or other irregularities. Of course, there are, also, other functions which can repair these errors. The user can also reduce the number of facets and smoother the surface.

5.1.4 Generation of the mesh

Meshing can be defined as the process of division or discretization of the model surface into the finite number of elements. The bigger number of elements, the higher accuracy of the results. However, the more elements, the more time is needed for the processing of the results. Meshing is important component of the analysis since the computation of the governing equation is based on the mesh. The governing equations are calculated again in every single element of the mesh. For every element of the mesh (in this master's thesis, the calculation is proceeded by means of Finite volume method) the value is calculated and the points between the elements are then interpolated; for more details see the chapter 3.3.1.

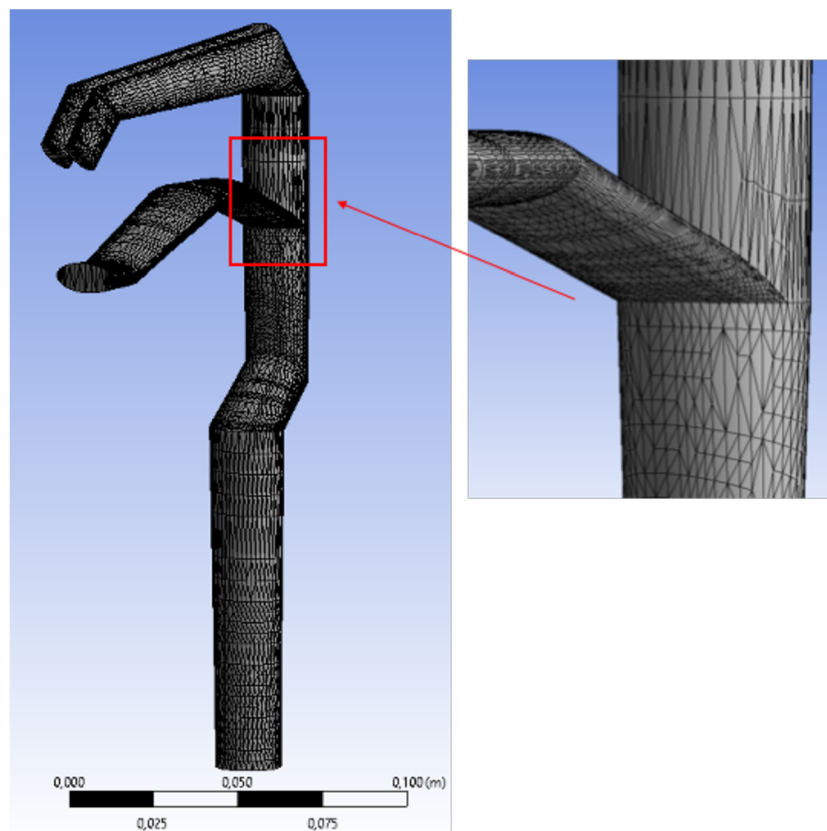


Figure 8: Illustration of the interface of Meshing

ANSYS Meshing is an internal part of the simulation process of ANSYS Workbench. This environment is automatically integrated with each solver and it chooses the most appropriate options based on the analysis type and geometry of the model. The example of Meshing is illustrated in figure 8.

For every model in the interface of ANSYS Meshing, the suitable method of meshing is provided. The user can choose from plenty of options according to the complexity and

geometry of the model. There is, also, possible, besides other, to choose the size of the meshing elements onto the part of the model or even onto the entire model, to enhance the accuracy of the meshing properties. There is load of other helpful functions used for creating quality and functional mesh for further processing.

In the Meshing interface, one other task is done besides the meshing itself: use of the function Named Selection. The function is used for naming all the individual parts of the model, so then during the analysis the software can recognize what are all the parts for. There must be the inlet (inlets), outlet (outlets) and walls determined.

5.1.5 Model Set up

After the preparation of the model, the analysis begins. It is focused on the pressure-based approach, since this approach is dealing with low speed incompressible flows of the air. The flow, in this master's thesis, is set to be mostly laminar, so the setting will be done according to this fact. Then, the material of the fluid has to be defined with the setting of the parameters – which can mean, for example, the viscosity of the fluid and density.

In Setup interface, very important part is to define Boundary conditions. Here it can be referred to the chapter 5.1.4, where the Named selection is described. This function will in particular help to define all the boundaries. In this section, the velocity of the flow through the pipe is determined. Very useful section is called Monitors, where there can be set the residual value. This value is mostly set to the very low number in order to increase solution accuracy. In this master's thesis all the analysis will be done with the residual value of $1e^{-6}$. The section Initialization is useful for setting the initial values.

Finally, in the section Run Calculation, the number of iterations has to be set. Again, applies the rule, that the more iteration, the more accuracy, but the more time consuming. The duration of the calculation differs also with the complexity of the model. Approximately, 100 iterations will consume few minutes if calculating the easy laminar flow pipe, but dozens of minutes if calculating the URT.

5.1.6 Numerical solution – contours

To see clearly the results, there are several options, how to depict them. The quickest way is to see first results already in the interface of Setup. For example, average velocity at the inlet and outlet can be checked, and so on. Better visibility, however, provides the interface of Results. Here it is possible to demonstrate the velocity magnitude of the flow, pressure distribution and others with the help of contours. Contours allows the user to plot lines and profiles superimposed on the physical domain. There is, of course, possible to choose any variable desired to depict.

5.1.7 Workflow of the analysis in ANSYS

Here, the diagram of the workflow in figure 9 is depicted for better understanding and easier summary of the entire workflow of the CFD analysis.

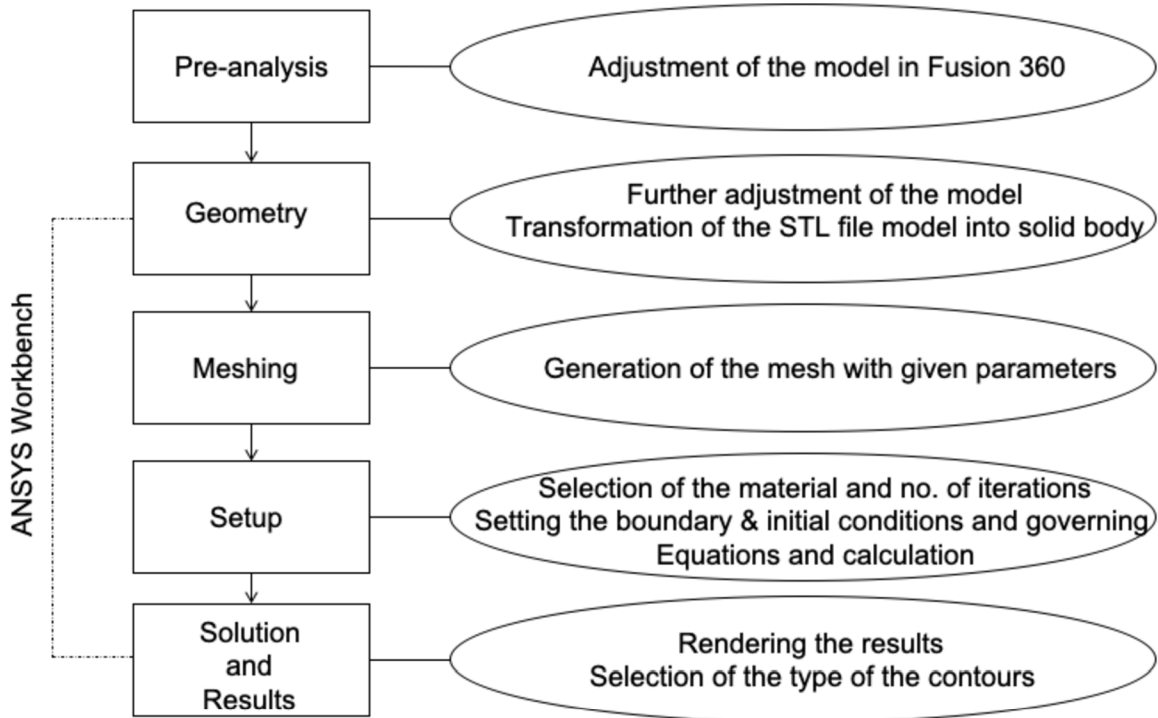


Figure 9: Diagram of the workflow of the CFD analysis

5.1 Choice of parameters

3D model of upper respiratory tract was processed in Engineering Simulation & 3D Design Software ANSYS Workbench, the student version Workbench 2019 and Workbench 2020 R1 was used. Ansys Workbench is an environment that aggregates the full spectrum of ANSYS simulation programs. For this thesis, the program ANSYS Fluent was used, which concerns the CFD analysis of the given model. This environment is in detail described above in the chapter 5.1.

The parameters used in this master's thesis were chosen based on the parameters in the papers written by A. F. Tena [1], T. B. Martonen [2] and E. Tsega [17] taken during inspiration.

INSPIRATION	Velocity (m/s)	Flow rate Q (L/min)	Pressure (Pa)		Density of air (kg/m ³)	Viscosity of air (kg/ms)	The number of iterations
A. F. Tena	-	15; 30; 75	-		-	-	-
E. Tsega	1,41	18,9	3,71		1,225	1,7894·10 ⁻⁵	-
T. B. Martonen	3,3 and 6,7	17 and 34	-		-	-	400

Table 1: The parameters of the variables used in fluid flow during inspiration

According to the table 1, the value for density of air and viscosity of air was chosen according to the article written by E. Tsega [17]. Also, the velocity value of 1,41 m/s was chosen from the same article for laminar flow. The flow rates are given accordingly.

In this master's thesis the value of viscosity used in the calculations is $\nu = 2 \times 10^{-5} \text{ m}^2 \text{ s}^{-1}$ and the value of density of air is $\rho = 1,2041 \text{ kg} \cdot \text{m}^{-3}$. Both values were calculated on the base of the equations mentioned earlier in this thesis.

6 Results

In this chapter, 2D model of the pipe flow was created, and further 3D model of the bend pipe flow, 3D reconstructed model of the original URT model was created, described and models were compared with each other. The propagation of the fluid velocity flow and pressure was realized using Navier-Stokes equations (Equation 5 and 12).

6.1 2D model of the cylindrical pipe

This chapter describes the settings of the parameters for implementation of the 2D model of the laminar air flow within the cylindrical pipe. Chapter consists of the description of the implementation of the geometry and mesh, choice of boundary conditions and initial conditions and registration of the governing equations. The purpose of this model is to understand how the analysis works and get familiar with all the properties and possibilities that modeling software ANSYS can offer.

6.1.1 Geometry and meshing

The cylindrical pipe was created in ANSYS DesignModeler, which is the program designed for creating and editing simple 2D and 3D geometries for CFD analysis, as mentioned in the chapter 5.1.2. The 2D pipe consists of two circular openings, connected by one cylindrical body. The pipe length and diameter does not correspond to the real size of URT since the purpose of the creation of this model is to understand the principle of CFD analysis.

It was determined to have rectangle structure and 100 divisions in the axial direction and 10 division in the radial direction; this means that the mesh consists of 1000 rectangle cells. In the Edge Sizing option, Hard Behavior was chosen, because it is very simple geometry.

The next step is to label boundaries in the Meshing interface. Assigning one opening as an inlet, another opening as an outlet and the body as a wall provides the determination of each part, so the analysis can move to the Setup interface as mentioned in the chapter 5.1.4.

6.1.2 Initial and boundary conditions, registration of the governing equation

After opening Setup, Double precision is selected, which means that it will use 64 bits for each floating-point number. This will increase precision for each number. Thereafter, the laminar flow is modelled with the inlet velocity 1 m/s since the aim of this analysis is to follow the most basic steps and get familiar with the environment. The fluid material is chosen as an air with such properties that the density is set to 1 kg/m^3 and the viscosity is $2e^{-3}$. Next step is to define the boundary conditions. In the Boundary condition option, the tube inlet is assigned as “Inlet-velocity”, tube outlet as “Outlet-pressure” and surface of the tube as “Wall”.

It is very important to do not forget to change the values in the option Monitors-Residuals, where the tolerances for the aggregate mass and momentum imbalances is set to the value of $1e^{-6}$.

At the end, the option Run Calculation is selected, where it is important to set number of iterations. Depending on the number of iterations, the accuracy of the calculation will change. The higher the number of iterations, the higher accuracy, but the calculation is more time consuming. So, the number of calculations was set to 1000.

6.1.3 Analysis and results

Velocity Magnitude Contours are the results visible on figure 10. It is a view of the longitudinal cross section through the pipe. We can see that on the left side of the pipe, vertically the place that we call inlet, has the green color, which indicates the velocity of 1 m/s. This is obvious, because such a velocity was set as initial condition. Further, it can be seen that in the middle of the pipe, where is seen red color, is the highest velocity and on the place very near inner wall of the pipe the velocity is coming to zero. This happens because of the inner friction, that is characterized by viscosity as mention in chapter 3.1.1.

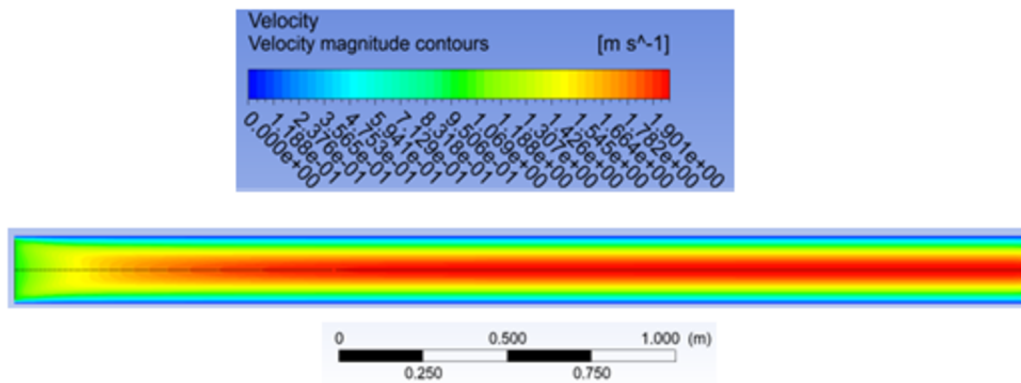


Figure 10: The propagation of the velocity magnitude within the pipe

Pressure Contours are the results visible on figure 11. It is, again, a view of the longitudinal cross section through the pipe. There is obvious loss of the pressure when progressing the pipe. On the left side, where there is an inlet, the pressure has the highest value (marked red) and it decreases towards the outlet. This phenomenon occurs since the air needs to be pushed through the tube. At the inlet, the pressure has the power to follow the air through the pipe, and at the outlet, since the air has the possibility to leave the pipe, the pressure decreases. This happened because of the physics rule: the fluid always flows from a higher-pressure point (higher pressure potential energy) to a lower pressure point (lower pressure potential energy).

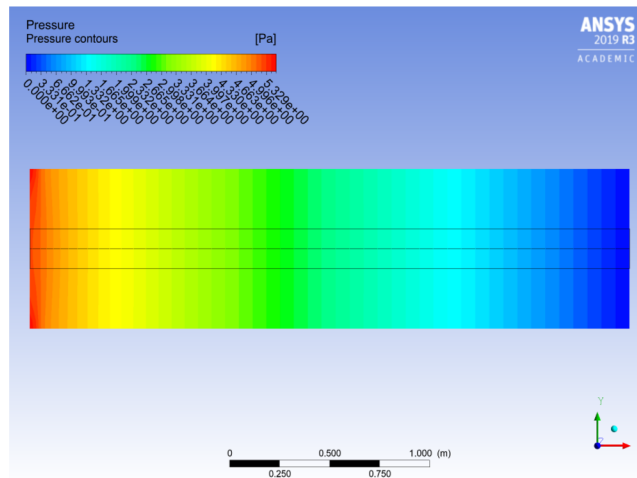


Figure 11: The distribution of the pressure within the pipe

The figure 12 shows how the velocity profile progress through the pipe. As it can be seen on the figure 10 of velocity magnitude contour, in the middle of the pipe the velocity vectors are gaining speed in comparison to the inlet and go towards the outlet. Since the velocity increases, the velocity profile is getting more rounded with the peak in the middle of the pipe. This phenomenon is more and more visible, the further is the fluid from the inlet and is described in the chapter 3.1.1 about viscosity. In the figure 12, we can, also, see the coloring of the velocity vectors. From this color information can be clearer how the velocity increases.

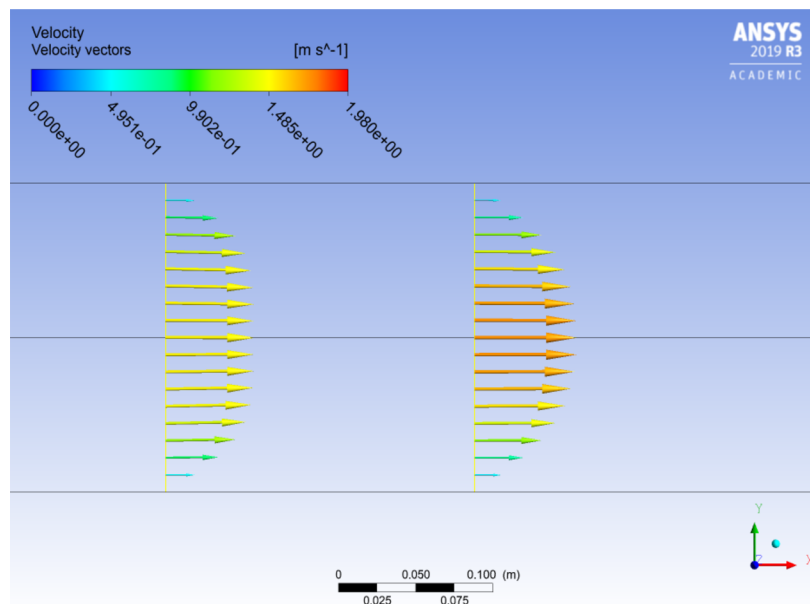


Figure 12: The velocity vectors of the moving fluid within the pipe

6.2 3D model of the laminar flow within the bend pipe

This chapter describes the settings of the components for implementation of the 3D model of the laminar flow within the simple bend pipe. The purpose of this model is to simulate the laminar flow inside the 90° bend pipe with given values of the variables. Air has been taken as the working fluid in this analysis.

6.2.1 Geometry and meshing

The geometry was designed in ANSYS SpaceClaim, which is described in chapter 5.1.2. Two circles with the same diameter and bend line was created and then by means of Sweep function the 3D bend pipe was constructed. The diameter of the inlet and outlet was 2 cm. The shorter part of the pipe is 10 cm and longer one has the length of 16 cm to approach the dimensions of the URT.

The geometry is divided into 3 mains parts: the longer part, shorter part and the curved part; to refine the mesh, it is possible to set the element size to different values in different parts. Therefore, the element size of the curved part was set to the value of 0,0005 m and other part were left as default value which was 0,001 m.

6.2.2 Initial and boundary conditions

The model is supposed to be laminar and viscous. The fluid, which is the medium inside the pipe, is planned to be air with the viscosity of $2 \cdot 10^{-5} \text{ kg/m} \cdot \text{s}$ and density of $2,2041 \text{ kg/m}^3$. For the boundary conditions, the end of the pipe on the shorter part of the pipe was assigned as an inlet and the end on the longer part of the pipe as an outlet. The velocity entering the inlet was $1,41 \text{ m/s}$. The number of iterations was set to 1000.

6.2.3 Analysis and results

On the figure 13 the velocity magnitude contour of the bend pipe with laminar flow is shown, with the initial velocity of $1,41 \text{ m/s}$. It can be seen, that the flow entering the pipe continues along the shorter part of the pipe with increasing velocity. Because of the inertial forces, the flow at the place of the bend tries to continue in its present motion, however the wall of the pipe does not allow this state. So, the flow accumulates on the more distant wall and continues down towards the outlet closer to the back wall, not completely in the middle of the pipe. The high velocity is illustrated by red color and low velocity by blue color.

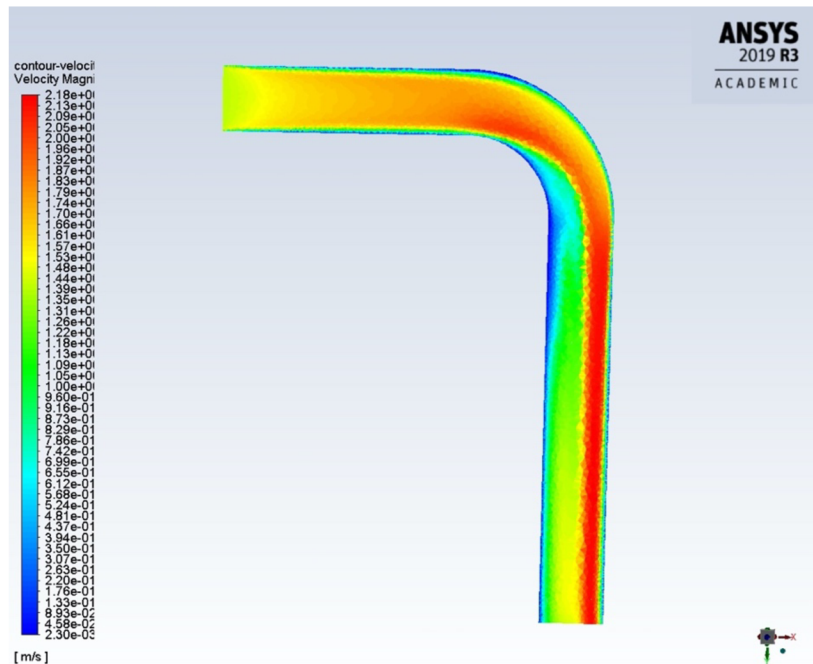


Figure 13: The velocity magnitude contour of the bend pipe

The figure 14 shows the pressure contour of the bend pipe. There is seen, that the pressure is very high at the inlet of the pipe. The reason is that the pressure helps move the air further into the pipe, as it was already explained in the chapter 6.1.3. Then, there is clearly visible another increase of the pressure exactly at the bend. This event is connected to what is explained in the paragraph above – the flow tends to continue horizontal but it not possible, therefore, the coming air pushes on the wall where a high pressure is created. The high pressure is illustrated by red color.

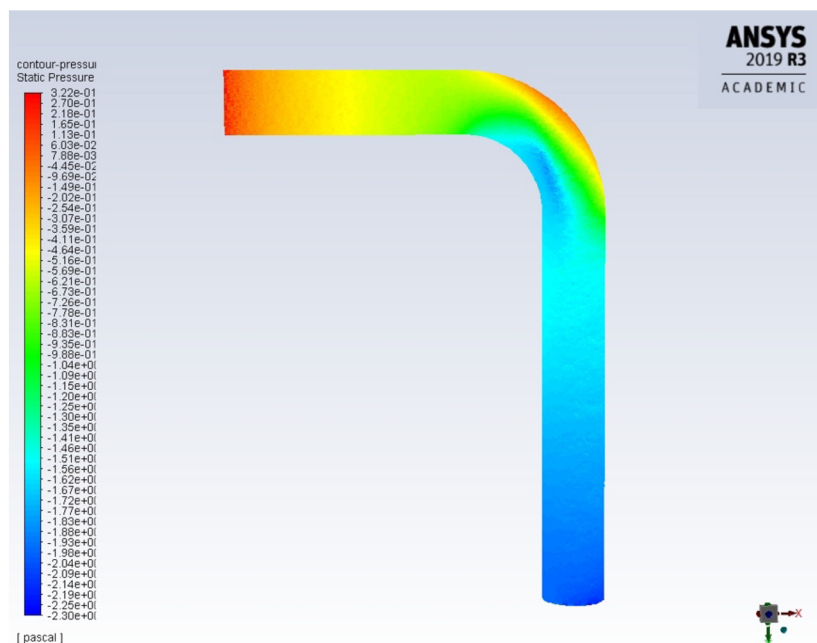


Figure 14: The pressure magnitude contour of the bend pipe

6.3 Simplified 3D model of the fluid flow

The following model was designed on the base of the original model segmented from the CT data. This model was proposed because of the impossibility of meshing of the original model made from CT data. Simplified URT was created in the software Fusion 360 described above. The original model was measured, and these values were applied on the simplified model, as it can be seen on the figure 16. In this master's thesis this model will be used throughout the rest of the thesis.

This chapter describes how the simplified model was created, furthermore a viscous, laminar flow of the air through URT under varying conditions will be presented, and the results of pressure and velocity characteristics will be evaluated.

6.3.1 Design of the model

This model was designed on the base of the original model from CT data. To create this model, it was a decision that was made after a lot of attempts to analyze the original model with the CFD software ANSYS. Because of hidden errors, there was no possibility to mesh the original model and therefore, it was not possible to analyze the data. Hence, the original model was measured to obtain the dimensions properties, such as the sizes of the cross-section area at specific places, especially in folds, also the distances between cross-section areas and degree of rotation of the cross-section area relative to the previous cross-section area. The pipe was created between each 2 areas, which is uniform in the diameter and has the length equal to provided distance. All dimensions properties can be found in the table 2 and the placement of the measurements on the figure 15.

Size of the cross-section area [mm]	Distance [mm]; degree [°]
D ₁ =19,2 x 19,0	V _{1,2} = 101,2; 0°
D ₂ = 25,1 x 14,9	V _{2,3} = 21,5; 45°
D ₃ = 20,7 x 17,2	V _{3,4} = 43,9; -45°
D ₄ = 20,7 x 17,2	V _{4,5} = 30,6; 65°
D ₅ = 26,1 x 8,1	V _{5,6} = 16,3; 25°
D ₆ = 26,1 x 8,1	V _{6,12} = 2,4; 25°
D ₇ = 20,7 x 17,2	V _{4,7} = 39,6; 0°
D ₈ = 20,7 x 20,7*	V _{7,8} = 12,7; 72,5°
D _{9a,b} = 6,0 x 18,2	V _{8,9} = 0
D ₁₀ = 5,1 x 16,6	V _{9,10} = 74,0; 65°
D ₁₁ = 7,6 x 13,6**	V _{10,11} = 19,3; 0°
D ₁₂ = 25,9 x 9,8	V _{12,13} = 40,0; 0°
D ₁₃ = 20,9 x 8,5	V _{13,14} = 10,0; -25°
D ₁₄ = 20,9 x 8,5	
*The plane of this area was shifted up by 8 mm.	
**The plane of this area was shifted front by 10 mm.	

Table 2: Overview of the model sizes

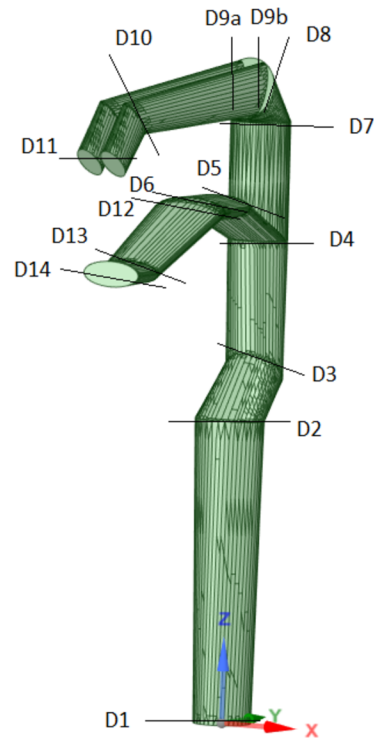


Figure 15: Schematic view of the simplified model with marked diameters

The simplified model was designed in Fusion 360 by means of basic Sketch and Measurement tools. The simplified model has 4199 faces, which is a big advantage of this model, since the computation is not so time demanding as it was in the original model, that has up to 1 million and 400 thousand faces.

The medium passing through URT is the viscous, Newtonian and incompressible fluid, referred as air. Every analysis was proceeded in CFD software ANSYS. Mesh was set to Patch conforming with the shape of tetrahedrons. The velocity of the flow in every single analysis is set to 1,41 m/s during inspiration through nose, as well as through the mouth, as mentioned in the chapter 5.1.

The number of iterations was set to 10.000. This number was the best compromise between the quality and time consumption. It was possible to afford higher number of iterations than it is mentioned in the table 1, since the model in particular article is much more complex and one iteration of that model takes much more time than it does in this master's thesis.

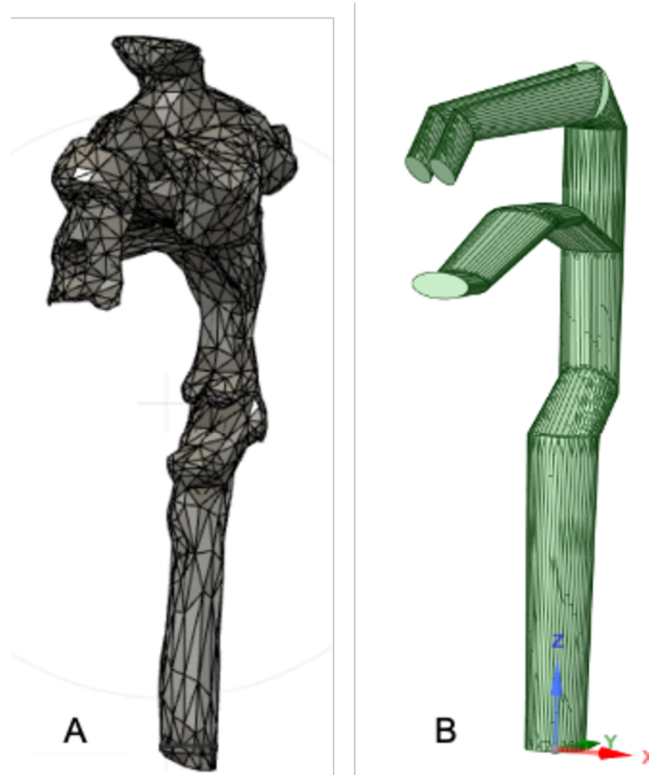


Figure 16: The comparison of the original (A) and simplified (B) model

6.3.2 The description of the individual model analyzes

In this chapter, the individual graphic model analysis results will be described in order to get a brief insight of how the models look like and how the velocity and pressure characteristics inside the model change when the conditions vary.

On the figure 17, the density inside the model is shown. As mentioned above, the density should be constant across the model. In this master's thesis, the value of $\rho = 2,2041 \text{ kg}/\text{m}^3$ was used. The figure 17 is a proof, that this fact was retained in the thesis and the density was really constant.

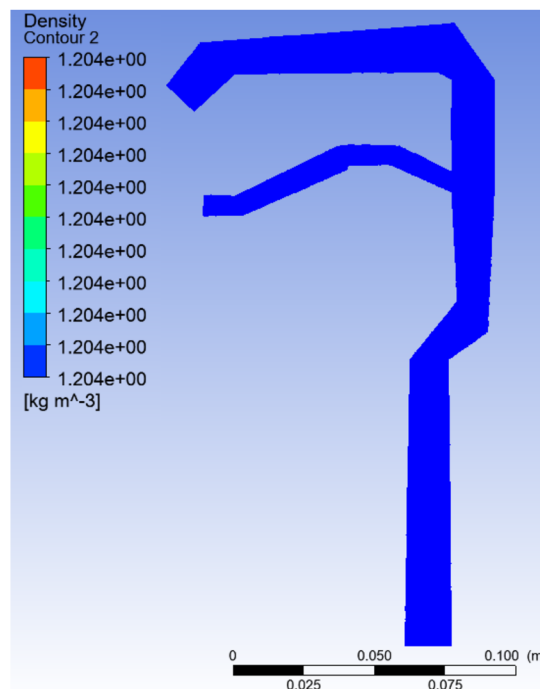


Figure 17: Density of the model

Characteristics of an air flow inhaled through the mouth and nose

Figure 18 shows the contours of velocity of the air flow inhaled into the model through the mouth and nose without any sampling gaps. On the part A, the cross section of the plane of the left nasal cavity is shown. It is obvious, that there are some turbulences in the first bend in the nasal cavity, when the air enters the nasal inlet. That can happen when the bend is too curved, and air has to change the direction. If the velocity is too high for slow adjustment of the flow to the bends, then vortexes and turbulent flow can occur there.

Part B shows the cross section through the median plane, which means the exact middle plane of the model. The difference between part A and part B is clear especially at the trachea, where the air flow in part B is much higher than in the part B. This fact is logical, since the flow in the middle of the tube should be the highest in comparison with the flow layers adjacent to the walls. This phenomenon is described in the chapter 3.1.1 above.

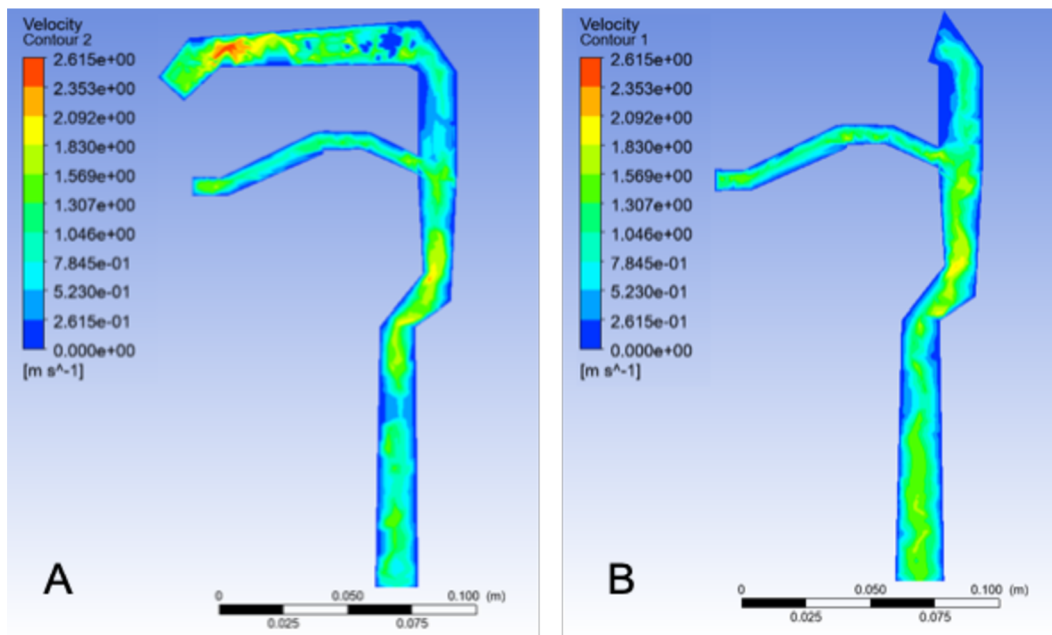


Figure 18: Velocity of the air flow inhaled through the mouth and nose, A: Cross section of the plane of the left nasal cavity, B: Cross section through the median plane

There is an illustration of the pressure distribution of the air flow inhaled through the nose and mouth on the figure 19. Part A, which is the plane crossing the left nasal cavity, shows, that there is an occurrence of the very high pressure, right at the nasal inlet. This phenomenon happens, because the air is pushed inside the nasal cavity and this creates higher pressure. This fact was already mentioned in the chapter 6.1.3. The slight increase in pressure, also, in the oral inlet in both, part A and part B can be seen. The pressure value is not as high as in the nasal inlet because the oral inlet diameter and diameter of the oral cavity is bigger than the nasal cavity is and therefore the air can pass more easily.

Another interesting location is at the lowest bend in the trachea, where the pressure drops to very low value. This occurs since the penultimate bend directs the flow to almost horizontal direction, then the flow tends to continue in the horizontal direction and hits the wall opposite the lowest bend of the trachea and therefore, the flow passes this bend without any closer contact. This causes the decrease of the pressure.

In the appendix of the master's thesis there are illustrated another two examples of the air flow inside the model without any sampling gaps. There can be found model where the air flow is inhaled only through the mouth (see figures 36, 37) and another where the air flow is inhaled only through the nose (see figures 38, 39). The differences between these three models are striking, since the flow inside the trachea is not grouped from two different flows (coming from the nasal and oral cavity), but the observer can easily track just one flow from the inlet till the outlet.

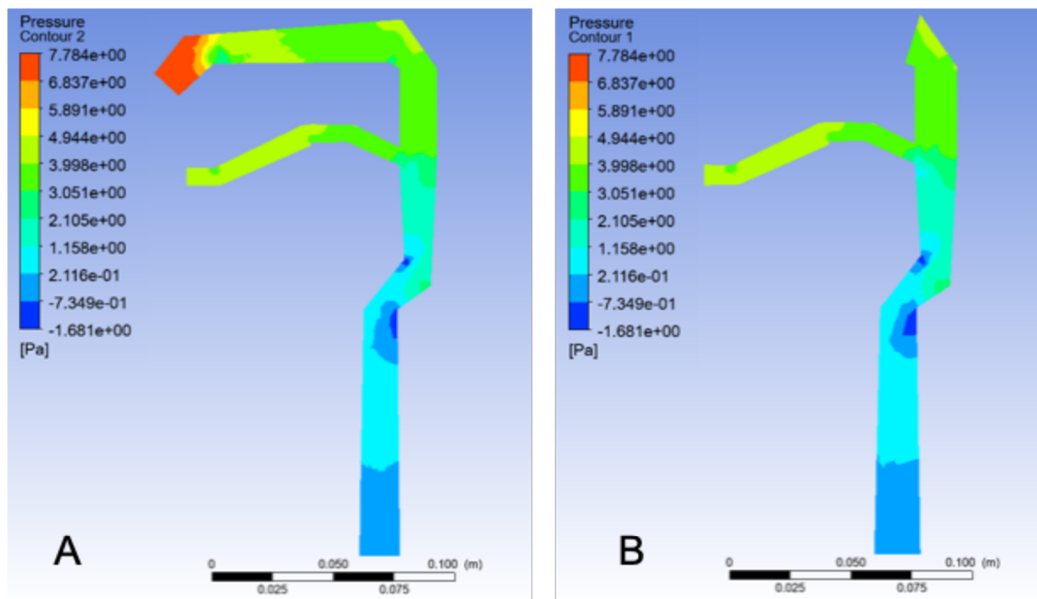


Figure 19: Pressure of the air flow inhaled through the mouth and nose, A: Cross section of the plane of the left nasal cavity, B: Cross section through the median plane

Characteristics of air flow inhaled through the mouth and nose with both sampling gaps

Figure 20 expresses the contours of velocity of the air flow inside the model equipped with two sampling gaps. The flow is going inside through the mouse and nose. In the part A of this picture, there is the plane of the left nasal cavity illustrated. There are the turbulences of the flow depicted in the first bend in the nasal cavity, which are already explained in the section above.

In the part B can be seen the sampling gaps placed on the back wall of the model. The velocity near the sampling gaps rapidly increases. It is clear that the velocity in the vicinity of the gap is higher at the lower sampling gap, because the velocity across the diameter at that spot is also higher. This happens because the flows from mouth and nose join and create even stronger flow.

Very interesting finding is also that the flow at the trachea runs much smoother than in the model without any sampling gaps mentioned above. This phenomenon is caused primarily due to the sampling gaps. Since the sampling gaps allow the air to exit the model, the air is divided and the pressure decreases, therefore, the air in the trachea is not pushed so hard to go further.

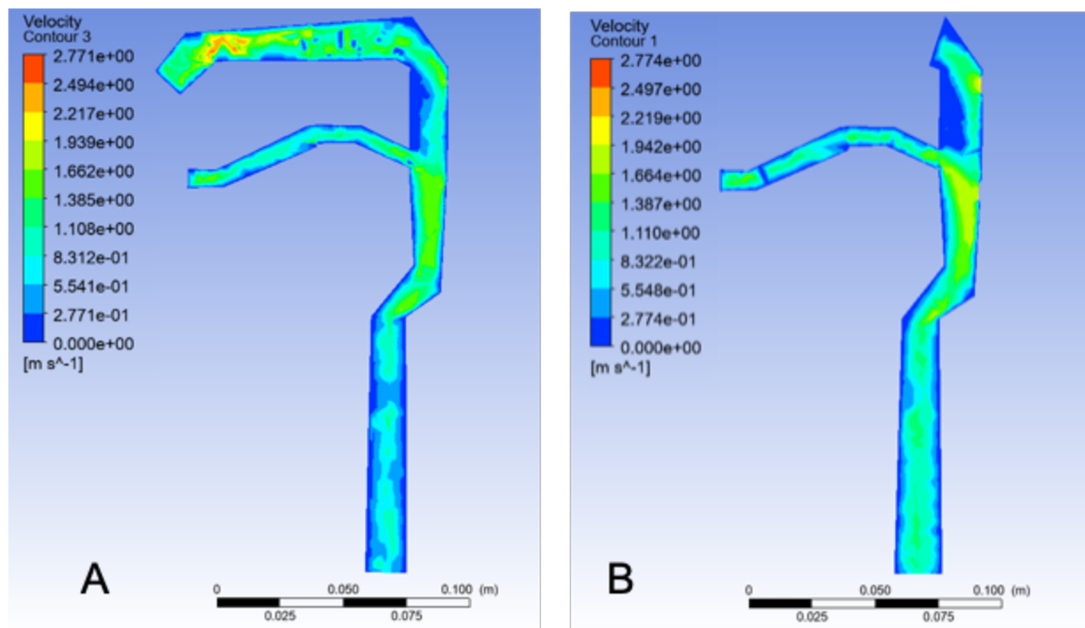


Figure 20: Velocity of the air flow inhaled through the mouth and nose with both sampling gaps, A: Cross section of the plane of the left nasal cavity, B: Cross section through the median plane

On the figure 21, in part A, the pressure of the air flow in the left nasal cavity is illustrated. There is obvious increase of the pressure at the nasal inlet and perceptible increase at the oral inlet. Very similar pressure contour is described in the model mentioned above. In the part B, it is shown, that the pressure decreases in the vicinity of the sampling gaps because, as mentioned before, the easier the air can flow in the given place, the lower is the pressure in there. Also, on both planes, there is clear drop of the pressure the lower the observer looks in the trachea. Since the air flow exits the URT, the pressure drops.

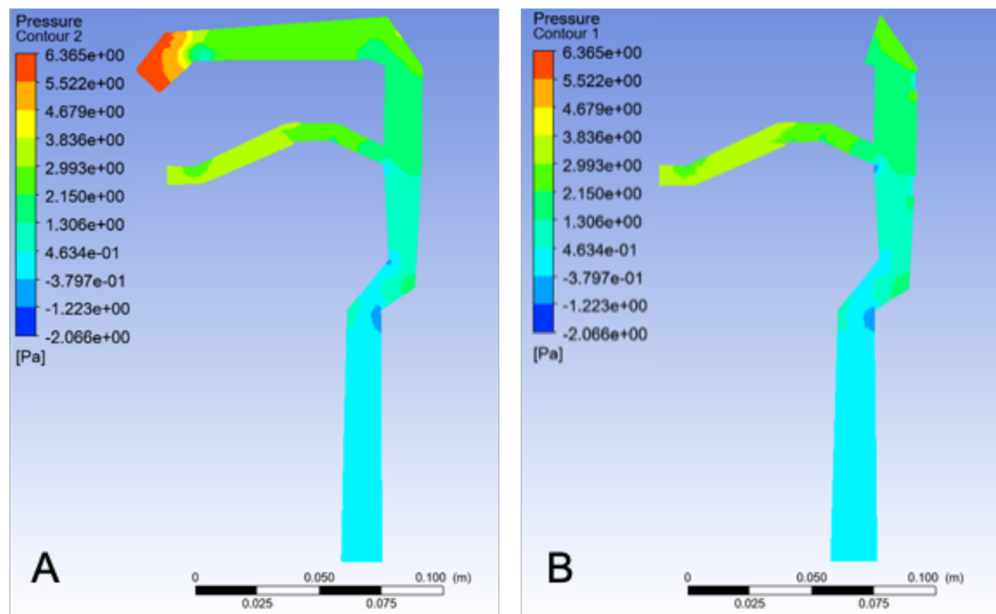


Figure 21: Pressure of the air flow inhaled through the mouth and nose with both sampling gaps, A: Cross section of the plane of the left nasal cavity, B: Cross section through the median plane

In the attachment the models of the air flow inhaled through the mouth and nose with first sampling gap (see figures 40, 41) and another model with second sampling gap (see figures 42, 43) can be found. There is shown, how the velocity and pressure change, if the air flow is forced to exit just through one gap. In that models, it will lead to the increase of the pressure in the neighborhood of the sampling gap.

Characteristics of air flow inhaled through the mouth with second sampling gap

Figure 22 explains, how the air flows, if inhaled just through the mouth. This model is equipped with one, lower, sampling gap. As it is mentioned above, the models, where the air is inhaled just through one inlet, can be more precisely trackable, since the flows does not join in the trachea. This model very clearly shows how the flow passes through the model.

Again, there are some turbulences on the first bend inside the oral cavity and some even smaller further this cavity. It is a normal phenomenon since the model has a lot of small bends. The highest velocity, however, can be found when the flow passes by the sampling gap. In the part B are the high velocity values marked red and are very clearly observable near the back wall of the model.

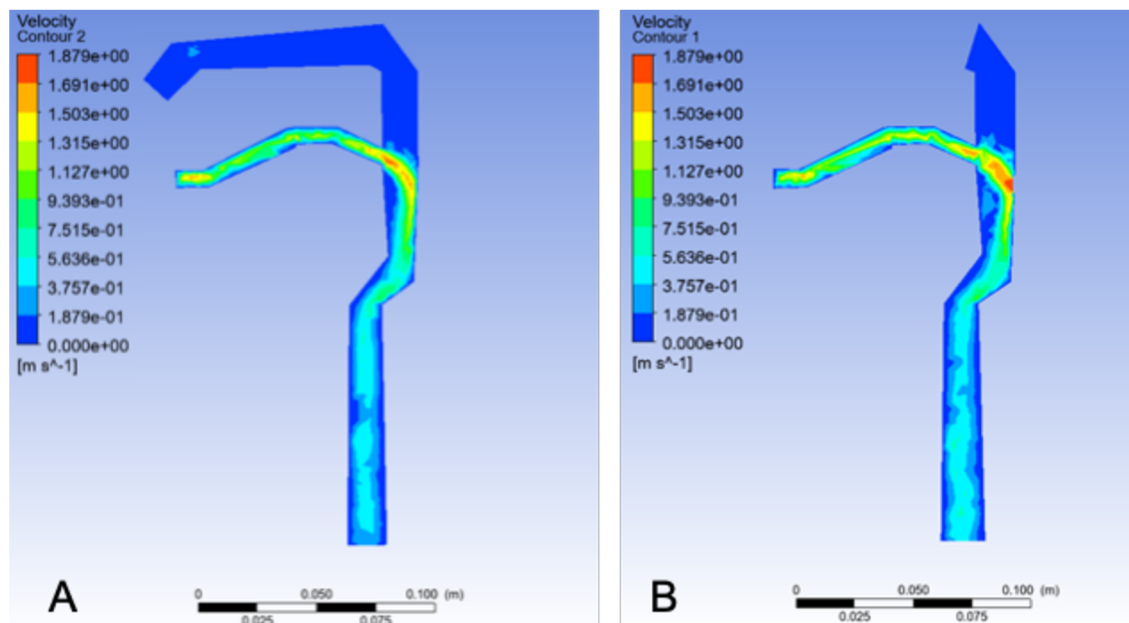


Figure 22: Velocity of the air flow inhaled through the mouth with the second sampling gap. A: Cross section of the plane of the left nasal cavity, B: Cross section through the median plane

By continuation of the previous paragraph, on the figure 23, there are visible 2 phenomena near the sampling gap. In the closest vicinity of the sampling gap, the pressure decreases, since the air flow leaves the model. However, in the neighborhood of the gap, the pressure seems little higher. This is caused by all the air flow trying to leave the model, but the diameter of the sampling gap is not as big as the amount of the air attempting to exit through the gap. The air is piled up near the sampling gap and this leads to the pressure increase.

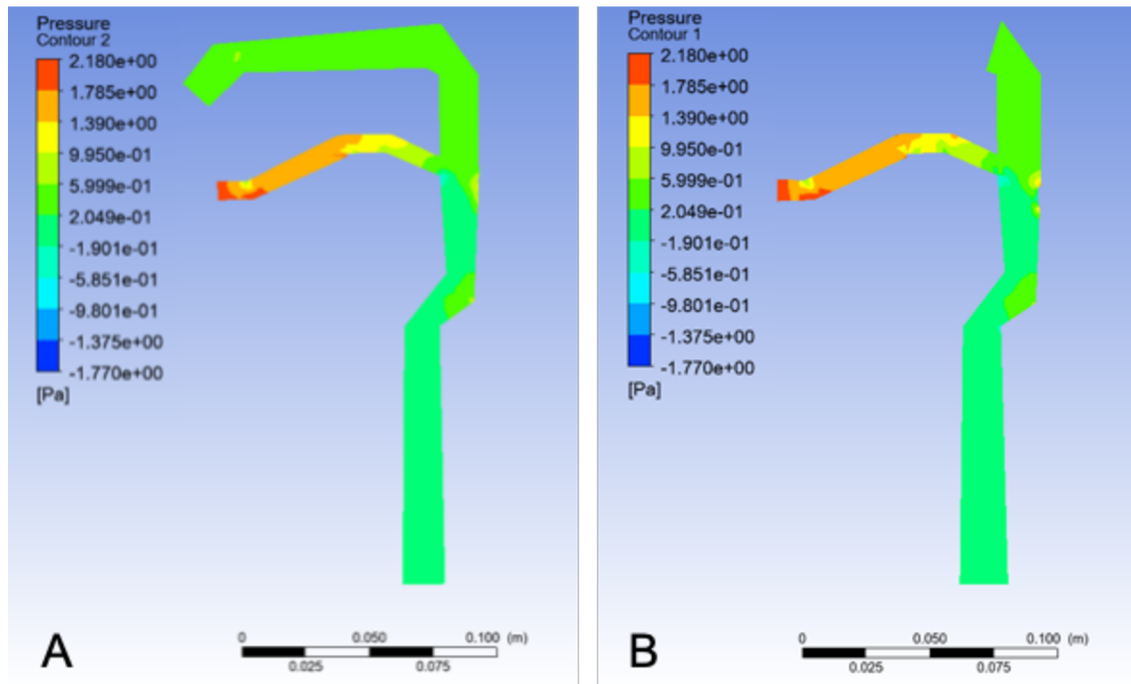


Figure 23: Pressure of the air flow inhaled through the mouth and nose with the first sampling gap, A: Cross section of the plane of the left nasal cavity, B: Cross section through the median plane

In the attachment, the observer can find, how the velocity and pressure characteristics behave if the air flow is inhaled only through the nose and can leave the model via first, upper, sampling gap (see figures 44, 45). The results are very similar, however not so obvious as in this model. Since the diameter of the oral cavity is bigger than the nasal cavity diameter, therefore, the amount of air entering the oral cavity is higher and hence, the flow is stronger with higher values, which can be then depicted during the analysis.

6.3.3 Analysis of the placement of the sampling gap

The main goal of this master's thesis is to find the best placement of the sampling gap at the surface of the model of URT. Here, the method of finding desired place is described and results of this method are determined.

For this analysis, 3 basic types of models are available:

- model with the air coming inside through the mouth and nose (Number 1),
- model with the air coming inside only through the mouth (Number 2), and
- model with the air coming inside only through the nose (Number 3),

which can be seen in the chapter 6.3.2 and in the attachment.

These three models were used in the first step in testing the comparison of the velocities at the place very near of the potential sampling gaps. Entire analysis workflow is shown on the figure 25. For each model identical 5 places were chosen, where 10 values of velocity at the same positions for each model were measured. Then, these values were proceeded in the analysis using statistical test ANOVA and paired t-test. By means of these tests, the best placement of the sampling gaps for the measurements by optical spectrometer can be determined. According to the visual evaluation, the 5 spots placed near the back wall of the model are chosen, as shown on figure 24.

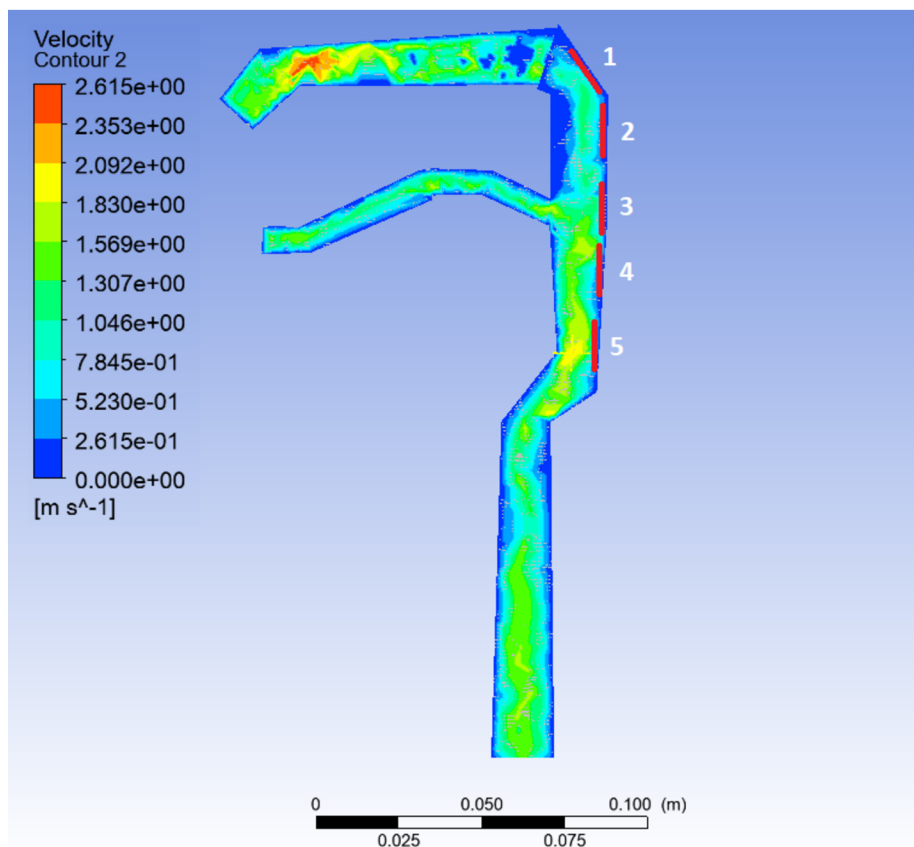


Figure 24: Placement of the possible sampling gaps for evaluation

Afterwards, in the second step, the best sampling gap according to the ANOVA test was created in the interface of ANSYS SpaceClaim and the analysis was proceeded again, already with physically present sampling gap. Using paired t-test, the values taken from the model without any gaps and the values taken from the model with designated points were compared and the changes were evaluated.

An additional comparison of the pressure characteristics was made using 10 pressure values from the model without any sampling gaps and 10 values from the model with the best sampling gap at the place of the sampling gap. The results are illustrated in the graphs for visual evaluation.

Testing of the analysis hypothesis

Since the analysis with ANOVA and paired t-test was done, the null H_0 and alternative H_1 hypothesis must be set, in order to confirm the results. The significance level was set to 0,05, which refers to the probability of rejecting the null hypothesis when it is true. Significance level of 0,05 indicates a 5% risk of concluding that a difference exists when there is no actual difference.

First step:

H_0 = There is not a difference between the 5 potential sampling gaps.

H_1 = There is a significant difference between the 5 potential sampling gaps.

Second step:

H_0 = There is not a difference between a potential sampling gap and a real sampling gap.

H_1 = There is a significant difference between a potential sampling gap and a real sampling gap.

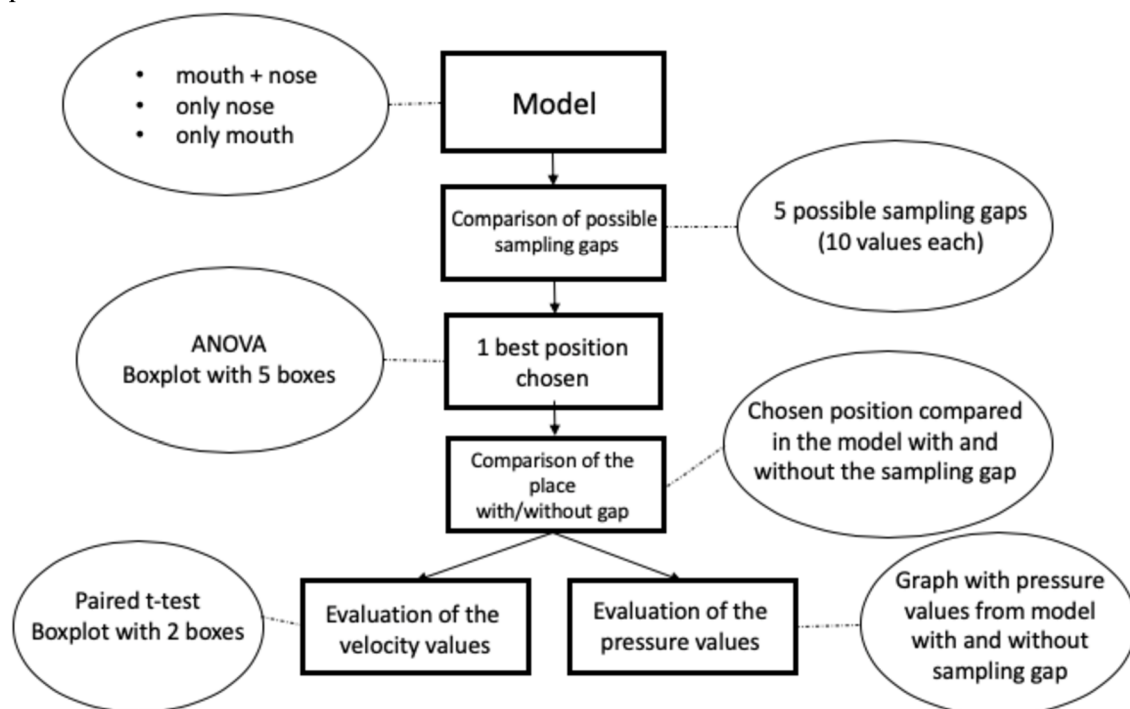


Figure 25: Diagram of the analysis workflow

Determination of the sampling gap in the model Number 1

Here it comes to the moment, where the best place for placement of the sampling gap will be determined. The highest velocities are compared at these places. The reason for this evaluation is, that these sampling gaps are to be used for the sampling and then analyzing by optical spectrometer. Of course, it is desirable to obtain good quality sample which passed from the mouth or nose inlet and directs to the outlet. To obtain such a sample, the best option is to create a sample from the moving air and that whole distribution of the particles of the air coming from the inlet will be provided in the sample.

Here, 10 velocity values were taken for every potential sampling gap very near to the potential sampling gap. In total, 50 values were taken. Afterwards, the ANOVA test was proceeded to determine best placed sampling gap. The ANOVA test determined, that the p-value in this test is $p = 6,17505 \cdot 10^{-23}$. It is obvious, that the p-value is very small number ($p < 0.05$), therefore the null hypothesis is rejected, and it means, that there is a significant difference between these 5 possible sampling gaps.

On the figure 26, the boxplot of the individual potential sampling gaps is shown, where the numbers of the sampling gaps correspond to the numbers shown on figure 24. As mentioned in the paragraph above, according to the results, the null hypothesis saying that all group means are equal, is rejected. Hence, it can be proved, that the highest velocity occurs close to the potential sampling gap number 4. Sampling gap number 4 is opposite the oral cavity.

At this moment, placement of sampling gaps is determined. The next step is to create sampling gap number 4 on the surface of the given model Number 1 and verify the previous results by providing another analysis. The values of velocity at the exact same place in the model without sampling gaps and also in the model with the chosen sampling gap were measured. Afterwards, the paired t-test analysis was done.

In the analysis using paired t-test, it was compared whether there is a difference in velocity on the place near sampling gap number 4 between the model without any sampling gaps and model with this sampling gap to see if the velocity distribution changed once the sampling gap is created.

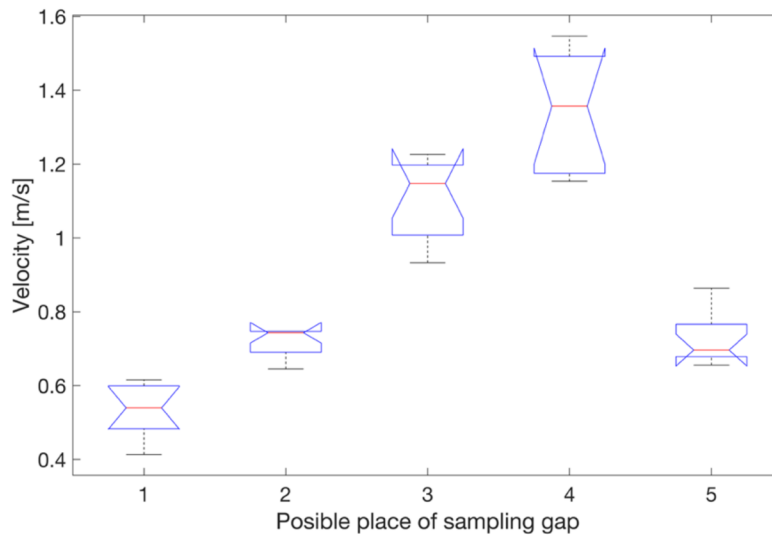


Figure 26: Boxplot of the results of the potential places of the sampling gaps in the model where the air is inhaled through the nose and mouth

The sampling gap number 4, according to the paired t-test, has the p-value, which is the significance level, $p = 1,33446 \cdot 10^{-05}$. It is higher than the statistical significance of 0,05. The null hypothesis, saying that there is no significant difference between a potential sampling gap and a real sampling gap, is rejected. Therefore, there is a difference.

In the figure 27, the two chosen spots are compared. On the x axes, the number 1 refers to the place in the model without any sampling gaps and number 2 refers to the model with the sampling gap number 4. It is depicted, that there is very expressive difference of the velocities between these places. According to the paired t-test the difference is significant. Therefore, it can be considered, that there are some changes inside the model once the sampling gap is created.

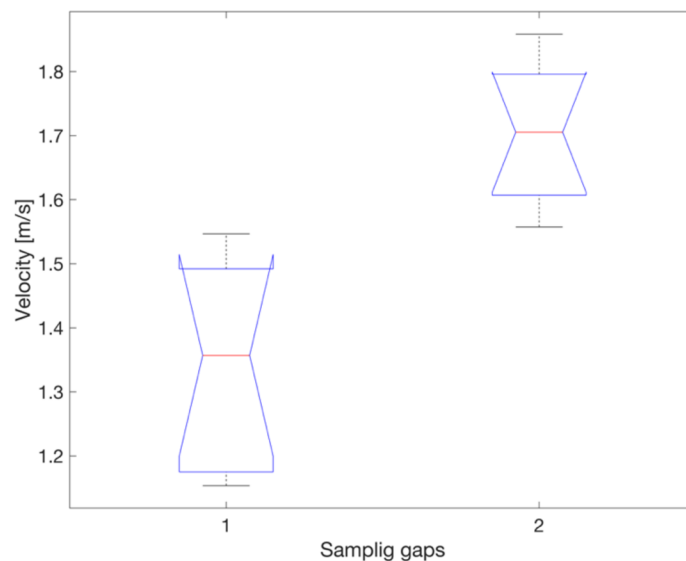


Figure 27: Boxplot of the comparison of the velocities at spot of sampling gap number 4 between the models where the air is inhaled through the nose and mouth with and without the sampling gap

Except for velocity distribution, also the pressure distribution can be determined. As it was already mentioned before in the master's thesis, there is a close relationship between the velocity and pressure inside the tube. It says that the lower the pressure, the higher the velocity is in the tube on the examined place. In this thesis, below on the figures 28, 31 and 34 is shown, that the velocity increase once the sampling gap is physically present in the model.

The values of pressure were measured on the exact same places as it was done for velocity. The pressure values were determined in the model without any sampling gaps and in the model with sampling gap number 4. On the figure 28, the graph of the pressure distribution in these two models is illustrated. 2 vectors including 10 values each are depicted, where the blue line shows the pressure vector of the values measured in the model without any sampling gaps and red line shows the pressure vector measured in the model with the sampling gap number 4.

When comparing the relation between the red and blue line, there is a significant drop of the pressure in the model with the sampling gap number 4. In this graph, the rule, saying the lower the pressure, the higher the velocity inside the tube, was proved.

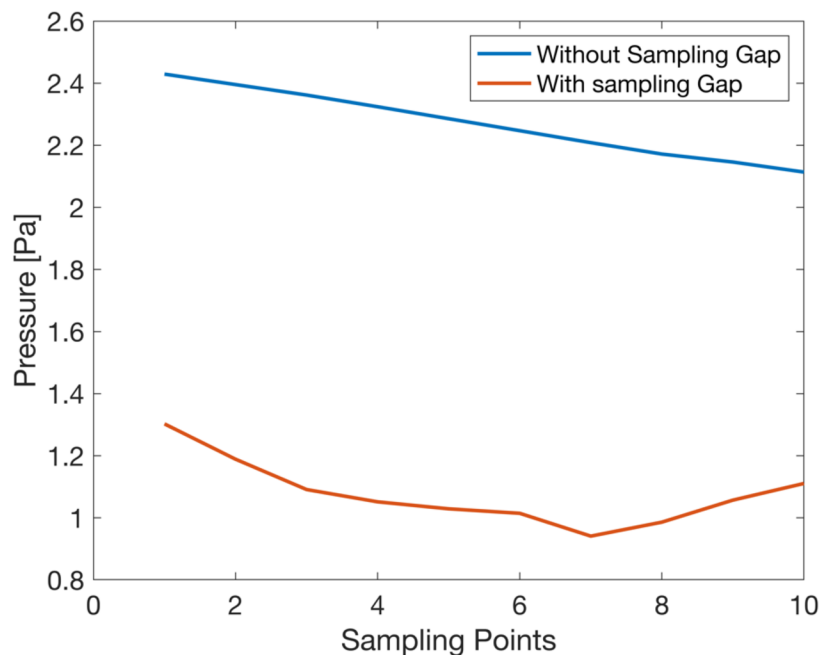


Figure 28: Pressure distribution in the model Number 1

Determination of the sampling gap in the model Number 2

In this analysis, the procedure will be completely the same as in the previous analysis, only with the difference, that the model will be switched to the model where the air is coming inside the URT only through the mouth. First step is to determine the best place for sampling gap. The places for placing potential sampling gap will remain the same as shown on the figure 24.

The statistical ANOVA test was provided with the p-value of $p = 1,33185 \cdot 10^{-44}$, which is really small value ($p < 0,05$), therefore the test rejects the null hypothesis saying that there is not a difference between the 5 potential sampling gaps. Therefore, it is confirmed that there is a significant difference between the potential sampling gaps in the model.

Figure 29 is a boxplot plotted with the median of the values marked red and whiskers at 25th and 75th percentiles. From the boxplot, it can be seen, that the place with the highest velocity is potential sampling gap number 4 and the result is really significant since the values of velocities of the potential sampling gap number 4 are much higher than of the other potential sampling gaps.

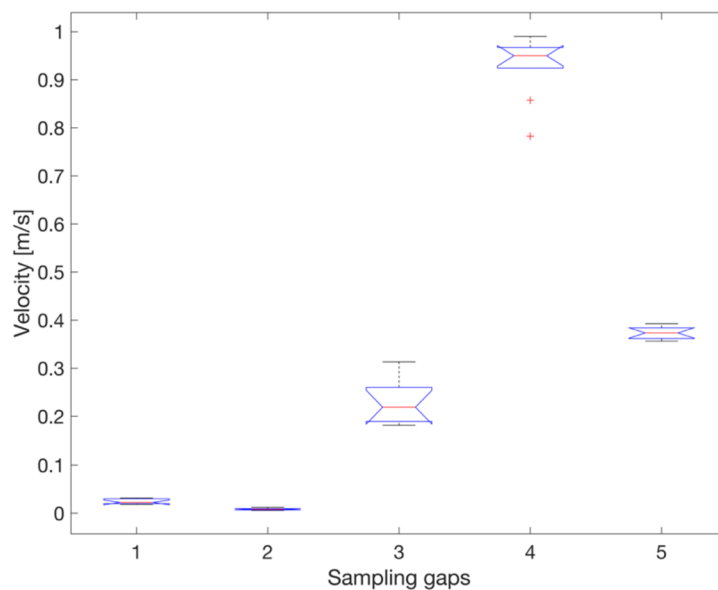


Figure 29: Boxplot of the results of the possible places of the sampling gaps in the model where the air is inhaled only through the mouth

The next step is to create the sampling gap exactly on the place of the potential sampling gap number 4. Then, the paired t-test analysis is done to find out, if there is a significant difference in velocities between a potential sampling gap and a real sampling gap.

Thanks to paired t-test the p-value was determined with the value of $p = 4,39426 \cdot 10^{-17}$. Because the p-value is very small ($p < 0,05$), the null hypotheses saying that there is no significant difference between a potential sampling gap and a real sampling gap, is rejected. This means that there is a difference and thus, it can be said, that the values differ if the sampling gap is added to the model. On the figure 30 the boxplot is depicted, where the first box refers to the place in the model without any sampling gaps and the second box refers to

the place in the model with the sampling gap number 4. There is clear difference between the values of these two places and it can be said that the velocity values and the results inside the model definitely change after providing the sampling gap number 4 to the model.

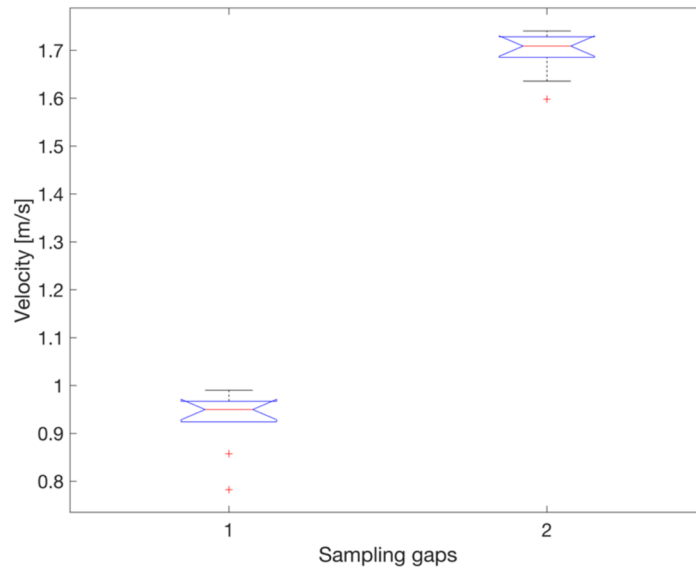


Figure 30: Boxplot of the comparison of the velocities at sampling gap number 4 between the models where the air is inhaled through the nose with and without the sampling gap

Figure 31 illustrates the pressure distribution depicted according to the same principle as it is shown in figure 28 and as it was already mentioned above. It can be seen that the drop of the pressure is perceptible and that the basic rule is proven in this model Number 2 as well. Ideally the pressure line is parallel with the horizontal axis, but, as mentioned above in this thesis, the pressure can increase in the neighborhood of the sampling gap. Sampling point number 1 is the highest point from all 10 points on the vertical axis and since the air flows down to the trachea, there is a possibility, that the air accumulates near the sampling gap before leaving the trachea and pressure increase on that place.

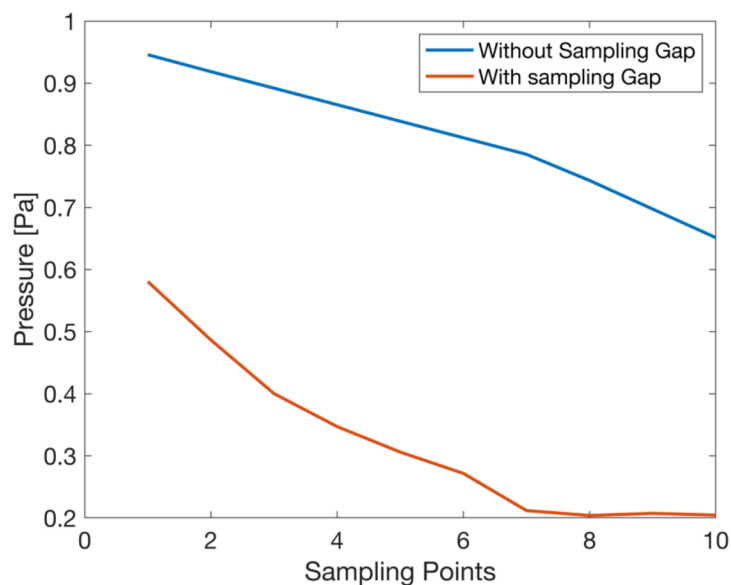


Figure 31: Pressure distribution in the model number 2

Determination of the sampling gap in the model Number 3

The last part of this analysis is to determine the best place for sampling gap in the model where the air is inhaled only through the nose and verify this assumption by further analysis. As in previous partitions of this analysis, the places of the potential sampling gaps were used, as shown in the figure 24. After completing the ANOVA test, the p-value is assigned to $p = 8,46843 \cdot 10^{-23}$. This p-value is much smaller than the significance level 0,05, which means that the null hypothesis is rejected and the difference between the 5 potential sampling gaps is significant.

On the figure 32 the boxplot with the potential sampling gaps on horizontal axes and with depicted values of velocities on the vertical axes is illustrated. Here, it can be said, that the best placement of the sampling gaps in this model is the sampling gap number 3. This finding is very interesting because the observer could think that the best place for placing the sampling gap will be number 1 or 2, since it is closer to the nose and therefore to the flow of the air leaving the nasal cavity.

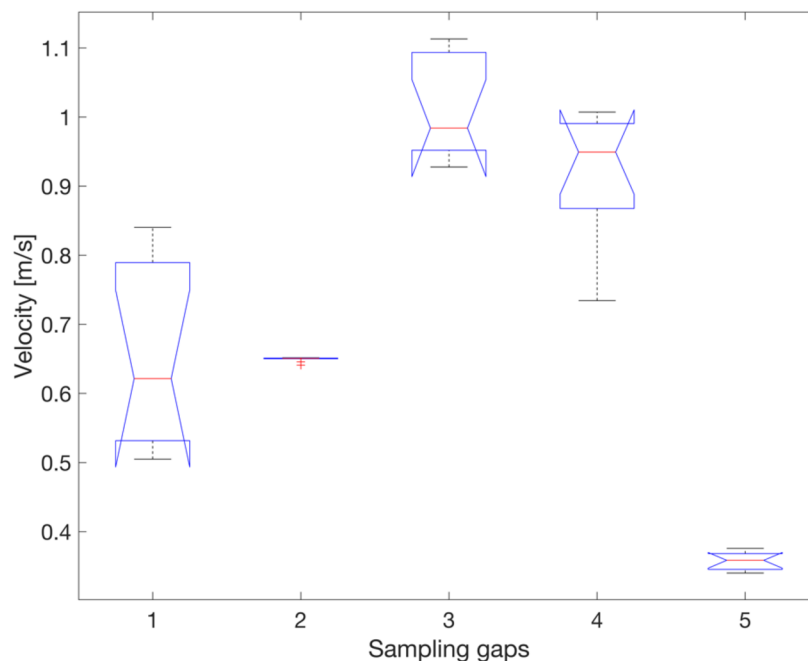


Figure 32: Boxplot of the results of the possible places of the sampling gaps in the model where the air is inhaled only through the nose

After the creation of the sampling gap number 3, the paired t-test was provided. The p-value was $p = 2,86894 \cdot 10^{-13}$, where ($p < 0,05$) suggests that the null hypothesis is rejected and therefore, there is a significant difference between a potential sampling gap and a real sampling gap. As shown, the figure 33 is a boxplot of the comparison of the velocities at sampling gap number 3 between the models where the air is inhaled through the nose without any sampling gaps and with the sampling gap. The first box represents the model without any sampling gaps and second box represents the model with sampling gap number 3. It can be clearly said, that there are changes in the distribution of velocity in the given place in the model with the sampling gap number 3 in comparison with the model without any sampling gaps.

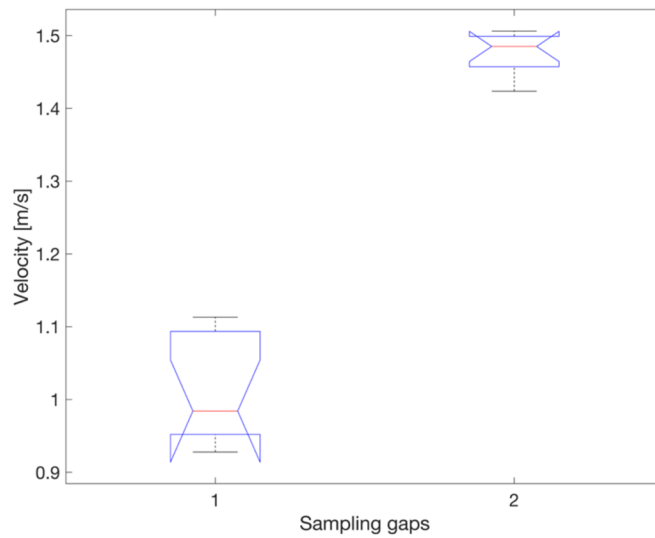


Figure 33: Boxplot of the comparison of the velocities at sampling gap number 3 between the models where the air is inhaled through the nose with and without the sampling gap

On the figure 34, there is a pressure distribution, where blue and red line is depicted referring to the vectors of pressure values measured in the model with the sampling gap number 3 (red line) and without the sampling gap (blue line). It can be seen, that there is a drop of pressure in the model with the sampling gap. Therefore, again, the applied rule saying that the lower pressure the higher velocity, was confirmed.

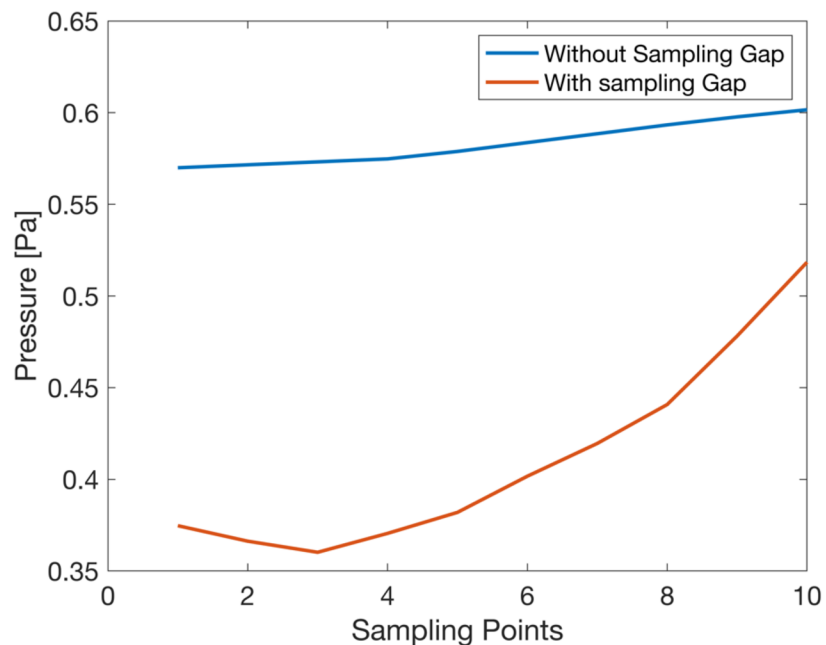


Figure 34: Pressure distribution of the model Number 3

6.3.4 Summary of results

Table 3 summarizes the results detailed in chapter 6.3.3. The column named Best sampling gap shows the best sampling gap according to the places assigned on the figure 24 which was determined by ANOVA test in the analysis. It is seen that model Number1 and model Number2 share the same position of the best sampling gap. It is given by the fact, that in these two models, the flow goes inter alia through the mouth inlet, therefore, this flow direct straight to the best sampling gap number 4. On the other hand, model Number3 allows the flow to go only through the nose, but the sampling gap number 4 is too far away to have the largest flow near sampling gap number 4 and so, the sampling gap number 3 it is.

The column called Value of velocity with sampling gap express, how the value of velocity changes after addition of the sampling gap to the model. It is clear that in each model the velocity greatly increases after sampling gap is added to the model. In the column named Value of pressure with sapling gap, the changes in the pressure value are shown. It is seen that the pressure decreases once the sampling gap is created within the model. It can be said, that the rule saying lower the pressure, the higher the velocity was proven in this analysis.

	Best sampling gap	Value of velocity with sampling gap	Value of pressure with sampling gap
Model Number1 (mouth + nose)	Number 4	↑	↓
Model Number2 (only mouth)	Number 4	↑	↓
Model Number3 (only nose)	Number 3	↑	↓

Table 3: Summary of the results

6.4 Particle deposition

This thesis, also, relates to the topic of particle deposition. It is topic, which can be taken as a superstructure or continuation of given topic of the entire master's thesis. First it is necessary to develop a reliable model and know all its characteristics. Then to determine the best sampling gaps and afterwards, the particle deposition can be simulated in order to find out further interesting findings about flow characteristics in relation to the particles.

This chapter deals with the simple model, where the simulation of particle deposition is shown. In this model the flow is inhaled only through the mouth and there is no sampling gap added. The initial condition for velocity of air flow is $v = 1,41 \text{ m/s}$, the same velocity has the injection of particles at the inlet. Also, gravity was taken in account with its value of $g = 9,81 \text{ m/s}^2$. The 10 different diameters of particles were chosen with the minimal diameter of $d_{min} = 1e^{-6} \text{ m}$, maximal diameter of $d_{max} = 2e^{-5} \text{ m}$ and mean diameter of $d_{mean} = 1e^{-5} \text{ m}$. The number of iterations were set to be 400 according to the paper written by T. B. Martonen [32], here the number of iteration did not have to be adjusted, since the computational complexity here is higher than when computing just the simplified model. The analysis was done with Discrete Phase, since the initial position, velocity and size was defined, and the Surface injection was chosen in order to be able to determine the inlet of the particles by mouth.

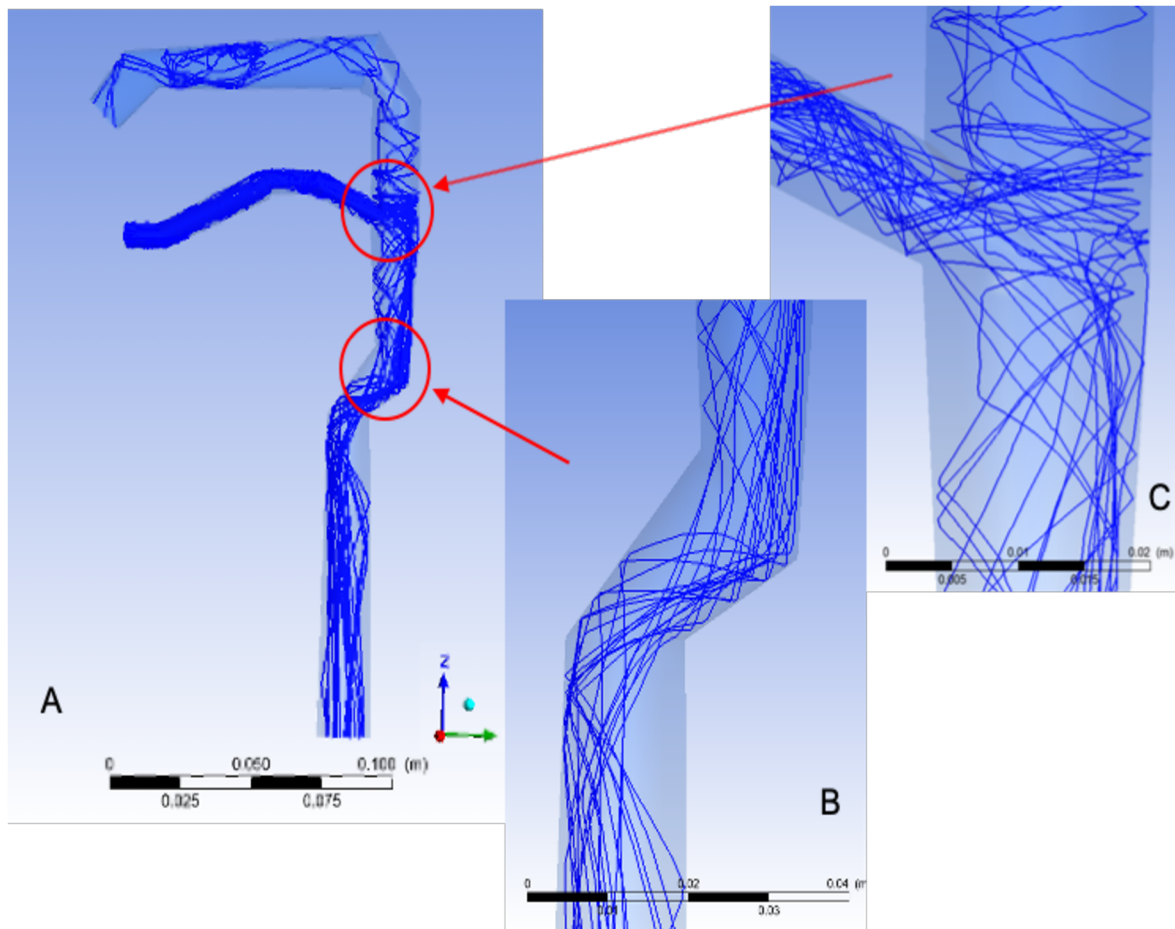


Figure 35: Trajectories of particles in the model, where the air and particles are inhaled only through the mouth

On the figure 35 the trajectories of the particles passing through the model can be seen. It is visible, how the particles hit the back wall when leaving the oral cavity, as seen in part C and then directing into the trachea. Some of the particles also aim into the nasal cavity. This is caused, because there is no air coming from the nasal inlet into the trachea and therefore, particles have a free passage in there. In the real human URT, for example in the case when asthma patient is inhaling the aerosol from inhalator, there would not be any particles entering the nasal cavity since the human can move the soft palate of the mouth and close the passage.

Very interesting moment is, also, when the particles are entering the trachea, as shown in part B. Because of the bends and curves, the particles bounce off the wall and aims to the opposite wall where they, again, bounce and then direct to the lungs.

Especially the phenomenon shown in part C is important for this thesis, since approximately on that place would be the sampling gap. As visible, particles are hitting the wall at the possible place of the sampling gap. After creating the sampling gap, it would lead into the sampling of the particles coming there.

7 Discussion

In this master's thesis, the 2D pipe and 3D bend pipe were created to outline the main principle of CFD modeling. Thereafter, the 3D model of URT realized from segmented CT data was created in order to provide analysis of velocity and pressure under varying conditions.

Firstly, the various combinations of varying conditions of the model were presented. The combinations included the models where the air flow was inhaled through the nose and mouth, the models where the air flow was inhaled only through the nose and the models where the air flow was inhaled only through the mouth. These situations were also divided depending on the quantity of the sampling gaps incorporated in the model. There could be no sampling gap involved in the model or there could be one sampling gap located on the upper place closer to the nasal cavity or on the lower place closer to the oral cavity, or the combination thereof. This analysis had mostly visual character. The following is a list of the greatest findings. On the illustrations it was found, that most of the results showed the small turbulences near the oral or nasal inlet. Initial condition for velocity was set to $1,41\text{ m/s}$, which with other conditions, such as density or viscosity, should provide laminar flow. Therefore, the turbulences probably occurred due to many small bends that the governing equations do not account for. Another interesting phenomenon happened near the outlet of sampling gaps. Right on the place adjacent to the sampling gap, the pressure decreases and therefore, the velocity rapidly increases. Since the sampling gap provides the free path for passage of the air out of the model, there is no wall to keep the pressure high and the air flow moves faster. Last but not least, when discussing the pressure shown on the pressure contours, it was always very high in value near the inlet of the mouth and the nose. It is caused because the flow needs to be pushed, in simple words, into the oral or nasal cavity in order to be moved further to the trachea. There is, also, seen, that the pressure was higher in the nasal cavity than in the oral cavity, which is caused by bigger diameter of the oral inlet than is the diameter of the oral inlets.

Secondly, the analysis using statistical tests ANOVA and pair t-test, was performed. The purpose of this analysis was to determine the best place for placing the sampling gap in each of the models described in the section 6.3.3 and verify the results. It was found out, that for the model where the air flow is inhaled through the mouth and nose the best place for sampling gap is the place slightly below the level of the oral cavity. This place is the best also for the model where the air flow is inhaled only through the mouth. This result was expected, since the flow going through the mouth and nose or going only through the mouth, is the strongest right below the level of the oral cavity. On the other hand, the best place for the model where the air flow is inhaled only through the nose is located right at the level of the oral cavity. This finding was very surprising, because the expected place of the sampling gap was at the level of the nasal cavity. This situation highlights the importance of the statistical tests, as it is more precise than visual evaluation.

During this analysis some major discoveries were also ascertained. On the base of the analysis by means of pair t-test it was determined, that the flow inside the trachea is much stronger in the model where the flow is inhaled through the mouth and nose than it is in the model where the air flow is inhaled only through the mouth or only through the nose. This

increase of velocity happens because when the air flows through the mouth and nose, the flows join together below the level of the oral cavity and create greater flow. The velocity, also, does not increase just in the trachea, but higher velocity was recorded also in the vicinity of the sampling gaps. It was determined that there is a great increase in velocity near the place of the sampling gap in the model where there is real sampling gap in comparison with the model where there is no sampling gap. As already explained herein, the velocity increases because the pressure near every single outlet decreases. This fact, of course, changes the characteristics of the flow inside the trachea, once the sampling gaps are created.

Pressure is also a variable, that manifests big changes in values, once the sampling gap is created in the model. According to the graphs shown in the Results section, there is a very big difference in pressure visible when comparing the model with or without the sampling gap. As it was already mentioned before, when the sampling gap is created, the pressure in the vicinity of the sampling gap decreases which then help the air to flow easier out from the model and therefore, the velocity increases.

Big issue discussed in all the research works dealing with modeling softwares is the number of iterations chosen for performing the analysis. As already mentioned, the more iterations selected, the higher become the time consumption of the process but also the more accurate the results will be.

During the development of the thesis, some of the limitations arisen. First of all, big limitation is the simplified model of URT realized from the model segmented from CT data. Originally, the scheme of the thesis was to perform analyzes on the model segmented from CT data. This model, however, was formed from 1 million and 400 thousand faces and student version of ANSYS Workbench allows to work just with maximum 5 thousand faces. Therefore, it was decided to create simplified model which shares the same dimensions properties as the original model segmented from CT data, but it has 4.199 faces in total. Afterwards, the analysis could be successfully completed. Another limitation of the simplified model is that the nasal cavity consists only from the tube referred as a nose, but the nasal cavities expanding above and behind the nose in the middle of the face are not included. This can cause some changes in the air flow.

In the future work, first suggestion would be to work with the improved version of ANSYS and provide the analysis with the original model segmented from CT data. Since the model covers the dimensions properties in detail of the URT of the patient, the model analyzes can be more accurate. This master's thesis is an ideal basis to continue with the analyses of particle deposition on CFD software. Even though, particle deposition has some research background, it is not completely examined on specific human-biological applications, such as modeling on URT. Further research of this area has several possibilities, for example on the medical industry, to model the interaction of inhaled medicaments for asthmatic patients. Another compelling modeling area is the epidemiological, by modeling the intercourse of virus and bacteria, on the respiratory tract. An additional example is the collusion model of external agents into the respiratory system, as health hazard. The information and results presented in this project can be used as a preamble to particle deposition research.

8 Conclusion

This master's thesis concerned the modeling of the velocity and pressure characteristics in the model of the human upper respiratory tract under varying conditions. These conditions include different placement and quantity of sampling gaps and choice of different combinations of inlets.

Theoretical part of the thesis described the anatomy and physiology of the upper respiratory tract and the mechanics of breathing. Further, the thesis was devoted to the computational fluid dynamics and the physics of fluid, which is very important in deeper understanding of the behavior of the fluids. Moreover, the CFD software ANSYS was described and, also, the theory of particle deposition.

Practical part concerned the creation of the 3D model of URT realized on the base of the segmented model from CT data and the CFD analysis was proceeded with this simplified model. The analysis included a generation of the simulation-appropriate mesh, a choice and an application of the CFD simulation boundary conditions and governing equations on given data. The results were presented and evaluated along with the illustrations of the models with different velocity and pressure characteristics.

Last but not least, the analysis of the combinations of the models under varying conditions was created, which contained the 3 different models without any sampling gaps participating in searching for the appropriate place for placement of the sampling gap. Further analysis using ANOVA and pair t-test was provided to verify the results. Besides other, it was found out, that the lower is the pressure, the higher become the velocity, especially near sampling gaps. Also, it was verified, that the pressure rapidly drops, once the sampling gap is created within the model.

This thesis aimed at examining a simple 3D model of URT under varying conditions. The extension of this thesis could be the research of particle deposition in the simplified or original model with given sampling points and further analysis in CFD software could be provided. The goal of this thesis was met, and interesting findings contributed to the research of CFD modeling of respiratory tract.

Bibliography

- [1] Tena A. F. and Clarà P.C., Use of Computational Fluid Dynamics in Respiratory Medicine, *Archivos de Bronconeumología* (english version), June 2015, pages 293-298
- [2] Martonen, T.B., Quan, L., Zhang, Z. et al. Flow simulation in the human upper respiratory tract. *Cell Biochem Biophys* 37, 27–36 (2002). <https://doi.org/10.1385/CBB:37:1:27>
- [3] Thibodeau G. A. and Patton K. T., *Anatomy & Physiology*, 6th ed., St. Louis, Mo.: Mosby Elsevier, 2007
- [4] Tortora G. J. and Nielsen M. T., *Principles of Human Anatomy*, 11th ed., Hooboken, N.J.: Wiley, 2008
- [5] Ellis H. and Mahadevan V., *Clinical Anatomy*, 13th ed., Chichester, West Sussex, UK: Wiley-Blackwell, 2013
- [6] Fusek, M. a Rojíček J., *Metoda konečných prvků I: Typy prvků*, Ostrava, 2013, ISBN 978-80-248-3023-0.
- [7] Jones J. G., *The upper airway*, London: Baillière, Tindall, 1995
- [8] Shier D., Butler J. and Lewis R., *Hole's Essentials of human anatomy and physiology*. 12th ed., New York: McGraw Hill, 2010
- [9] Patwa A, Shah A. Anatomy and physiology of respiratory system relevant to anaesthesia. *Indian journal of Anaesthesia*. 2015; 59(9): 533–541. doi: 10.4103/0019-5049.165849
- [10] Brandwein-Gensler M. S., Mahadevia P. and Gnepp D. R., „Nonsquamous Pathologic Diseases of the Hypopharynx, Larynx, and Trachea“, *Diagnostic Surgical Pathology of the Head and Neck*, 2nd ed., Elsevier, 2009, Pages 309-411
- [11] Shiba T. L. and Chhetri D. K., „Oropharynx“, *Disphagia Evaluation and Management in Otolaryngology*, Elsevier, 2019, Pages 13-21
- [12] Pocock G. and Rochards Ch. D., *Human Physiology: The Basics of Medicine*, 2nd ed., Oxford: OUP Oxford, 2004
- [13] Ferziger J. H., Peric M., *Computational Methods for Fluid Dynamics*, 3rd ed., New York: Springer, Berlin, Heidelberg, 2002
- [14] Tu J., Yeoh G. H. and Liu Ch., *Computational Fluid Dynamics*, 3rd ed., ScienceDirect, 2019, doi: <https://doi.org/10.1016/C2015-0-06135-4>
- [15] Cobelli C. and Carson E., *Introduction to modeling in physiology and medicine*, Elsevier, 2008
- [16] Bastian E. R., *Microfluidics: Modeling, Mechanics and Mathematics*, 1st ed., Elseier, 2017, doi: <https://doi.org/10.1016/C2012-0-02230-2>

- [17] Tsega, Endalew. (2018). Computational Fluid Dynamics Modeling of Respiratory Airflow in Tracheobronchial Airways of Infant, Child, and Adult. *Computational and Mathematical Methods in Medicine*. 2018. 1-9. 10.1155/2018/9603451.
- [18] Habaj E., Studium proudění tekutin pomocí programu COMSOL Multiphysics, České Budějovice, Bachelor thesis, University of South Bohemia in České Budějovice
- [19] Fanchi J. R., *Shared Earth Modeling*, 1st ed., Elsevier, 2002, doi: <https://doi.org/10.1016/B978-0-7506-7522-2.X5000-9>
- [20] Batchelor G. K., *An Introduction to Fluid Dynamics*, 1st ed., Cambridge University Press, 2001
- [21] Moukalled F., Mangani L. and Darwish M., *The Finite Volume Method in Computational Fluid Dynamics*, 1st ed., 2016, doi: <https://doi.org/10.1007/978-3-319-16874-6>
- [22] Matsson J., *An Introduction to ANSYS Fluent 2019*, 1st ed., SDC Publications, 2020
- [23] Viswanath D. S., Ghosh T. K., Prasad D. H. L., Dutt N. V. K. and Rani K. Y., *Viscosity of liquids: Theory, Estimation, Experiment, and Data*, 1st ed., Springer, Dordrecht, 2007, doi: <https://doi.org/10.1007/978-1-4020-5482-2>
- [24] Trefil J. S., *Introduction to the Physics of Fluids and Solids*, 1st ed., Pergamon Press, 1975
- [25] Ward-Smith J., *Mechanics of Fluids*, 9th ed., UK: Spon Press, 2011
- [26] Dhanani, Jayesh & Fraser, John & Chan, Hak-Kim & Rello, Jordi & Cohen, Jeremy & Roberts, Jason. (2016). Fundamentals of aerosol therapy in critical care. *Critical Care*. 20. 10.1186/s13054-016-1448-5.
- [27] Finlay W. H., „Particle deposition in the respiratory tract“, *The mechanics of Inhaled Pharmaceutical Aerosols*, 2nd ed., ScienceDirect, 2019, Pages 133-182
- [28] Agranovski I., *Aerosols – Science and Technology*, 1st ed., Wiley-VCH Verlag GmbH & Co. KGaA, 2010
- [29] Ruzer L. S. and Harley N. H., *Aerosols Handbook: Measurement, Dosimetry, and Health Effects*, CRC Press, 2004
- [30] Versteeg H. K. and Malalasekera W., *An Introduction to Computational Fluid Dynamics: The finite volume method*, 2nd ed., England: Pearson Education Limited, 2007
- [31] Tu J., Yeoh G. H. and Liu Ch., *Computational Fluid dynamics: A Practical Approach*, 1st ed., UK: Elsevier, 2008
- [32] Martonen T. B., Zhang Z., Yue G. and Musante C. J., *3-D Particle transport within the human upper respiratory tract*, Elsevier, 2002

List of Figures

Figure 1: Anatomy of the upper respiratory tract [8]	10
Figure 2: Anatomy of lower respiratory tract [8]	11
Figure 3: The partition of the velocities of the fluid depending on the distance from the pipe wall [24]	14
Figure 4: Velocity distribution in laminar flow of the fluid [18]	15
Figure 5: Velocity distribution in laminar flow of the fluid [18]	15
Figure 6: Division of the flow domain with extra nodes added [13]	19
Figure 7: Illustration of different mechanisms of particle deposition [26]	21
Figure 8: Illustration of the interface of Meshing	23
Figure 9: Diagram of the workflow of the CFD analysis	25
Figure 10: The propagation of the velocity magnitude within the pipe	28
Figure 11: The distribution of the pressure within the pipe	29
Figure 12: The velocity vectors of the moving fluid within the pipe	29
Figure 13: The velocity magnitude contour of the bend pipe	31
Figure 14: The pressure magnitude contour of the bend pipe	31
Figure 15: Schematic view of the simplified model with marked diameters	32
Figure 16: The comparison of the original (A) and simplified (B) model	33
Figure 17: Density of the model	34
Figure 18: Velocity of the air flow inhaled through the mouth and nose, A: Cross section of the plane of the left nasal cavity, B: Cross section through the median plane	35
Figure 19: Pressure of the air flow inhaled through the mouth and nose, A: Cross section of the plane of the left nasal cavity, B: Cross section through the median plane	36
Figure 20: Velocity of the air flow inhaled through the mouth and nose with both sampling gaps, A: Cross section of the plane of the left nasal cavity, B: Cross section through the median plane	37
Figure 21: Pressure of the air flow inhaled through the mouth and nose with both sampling gaps, A: Cross section of the plane of the left nasal cavity, B: Cross section through the median plane	37
Figure 22: Velocity of the air flow inhaled through the mouth with the second sampling gap, A: Cross section of the plane of the left nasal cavity, B: Cross section through the median plane	38
Figure 23: Pressure of the air flow inhaled through the mouth and nose with the first sampling gap, A: Cross section of the plane of the left nasal cavity, B: Cross section through the median plane	39
Figure 24: Placement of the possible sampling gaps for evaluation	40
Figure 25: Diagram of the analysis workflow	41
Figure 26: Boxplot of the results of the potential places of the sampling gaps in the model where the air is inhaled through the nose and mouth	43
Figure 27: Boxplot of the comparison of the velocities at spot of sampling gap number 4 between the models where the air is inhaled through the nose and mouth with and without the sampling gap	43
Figure 28: Pressure distribution in the model Number 1	44
Figure 29: Boxplot of the results of the possible places of the sampling gaps in the model where the air is inhaled only through the mouth	45

Figure 30: Boxplot of the comparison of the velocities at sampling gap number 4 between the models where the air is inhaled through the nose with and without the sampling gap.....	46
Figure 31: Pressure distribution in the model number 2.....	46
Figure 32: Boxplot of the results of the possible places of the sampling gaps in the model where the air is inhaled only through the nose.....	47
Figure 33: Boxplot of the comparison of the velocities at sampling gap number 3 between the models where the air is inhaled through the nose with and without the sampling gap.....	48
Figure 34: Pressure distribution of the model Number 3.....	48
Figure 35: Trajectories of particles in the model, where the air and particles are inhaled only through the mouth.....	50
Figure 36: Velocity of the air flow inhaled through the mouth, A: Cross section of the plane of the left nasal cavity, B: Cross section through the median plane.....	61
Figure 37: Pressure of the air flow inhaled through the mouth, A: Cross section of the plane of the left nasal cavity, B: Cross section through the median plane.....	61
Figure 38: Velocity of the air flow inhaled through the nose, A: Cross section of the plane of the left nasal cavity, B: Cross section through the median plane.....	62
Figure 39: Pressure of the air flow inhaled through the nose, A: Cross section of the plane of the left nasal cavity, B: Cross section through the median plane.....	62
Figure 40: Velocity of the air flow inhaled through the mouth and nose with first sampling gap, A: Cross section of the plane of the left nasal cavity, B: Cross section through the median plane.....	63
Figure 41: Pressure of the air flow inhaled through the mouth and nose with the first sampling gap, A: Cross section of the plane of the left nasal cavity, B: Cross section through the median plane.....	63
Figure 42: Velocity of the air flow inhaled through the mouth and nose with the second sampling gap, A: Cross section of the plane of the left nasal cavity, B: Cross section through the median plane.....	64
Figure 43: Pressure of the air flow inhaled through the mouth and nose with the second sampling gap, A: Cross section of the plane of the left nasal cavity, B: Cross section through the median plane.....	64
Figure 44: Velocity of the air flow inhaled through the nose with the first sampling gap, A: Cross section of the plane of the left nasal cavity, B: Cross section through the median plane.....	65
Figure 45: Pressure of the air flow inhaled through the nose with the first sampling gap, A: Cross section of the plane of the left nasal cavity, B: Cross section through the median plane.....	65

List of Tables

Table 1: The parameters of the variables used in fluid flow during inspiration	26
Table 2: Overview of the model sizes	32
Table 3: Summary of the results	49

List of Abbreviations

ANOVA	Analysis of Variance
ANSYS	Analysis System
CFD	Computational Fluid Dynamics
CT	Computed Tomography
FDM	Finite difference method
FEM	Finite element method
FVM	Finite volume method
URT	Upper respiratory tract

A: Figures of modelled characteristics of the air flow under varying conditions

Characteristics of air flow inhaled through the mouth

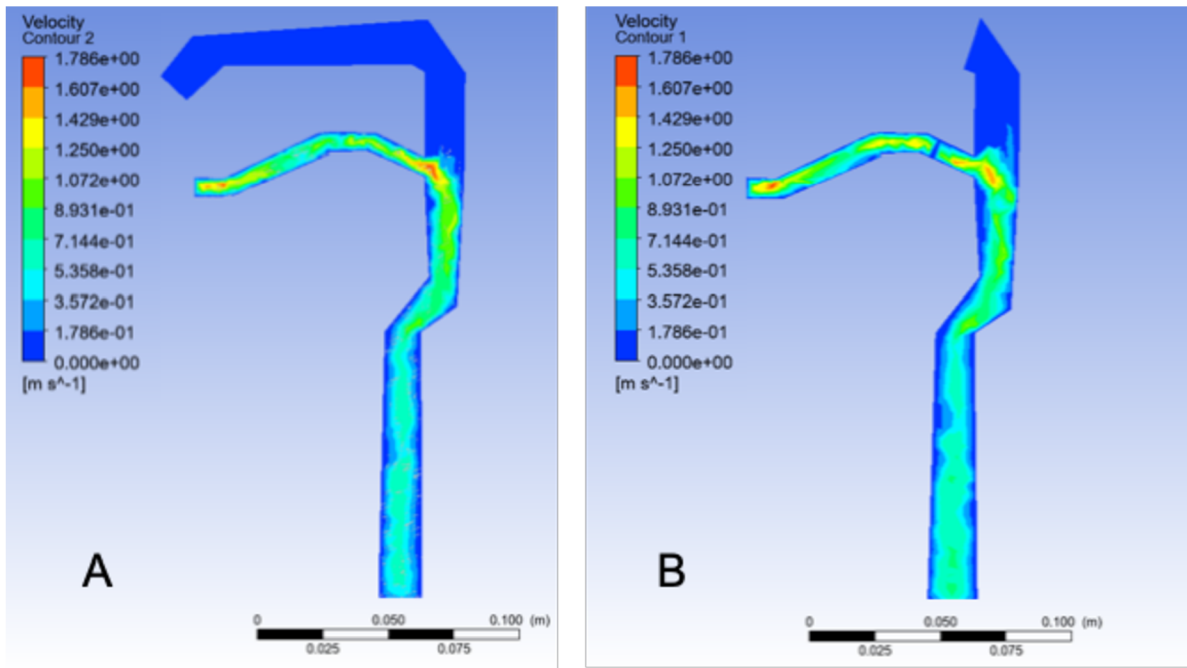


Figure 36: Velocity of the air flow inhaled through the mouth, A: Cross section of the plane of the left nasal cavity, B: Cross section through the median plane

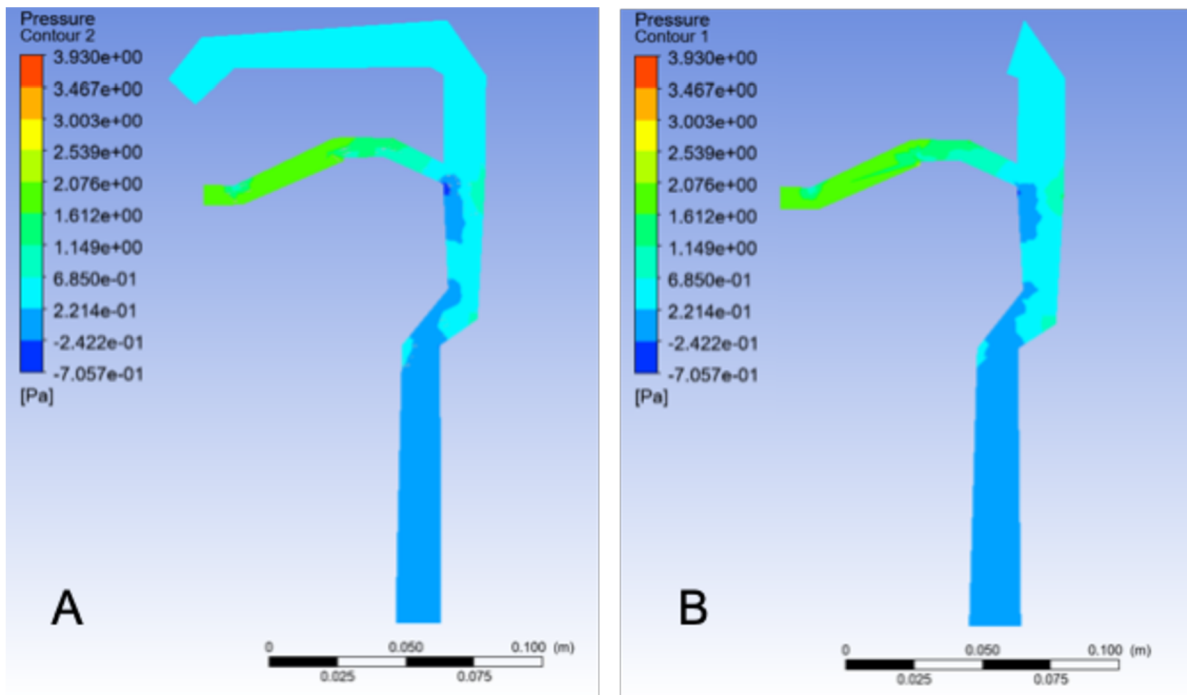


Figure 37: Pressure of the air flow inhaled through the mouth, A: Cross section of the plane of the left nasal cavity, B: Cross section through the median plane

Characteristics of air flow inhaled through the nose

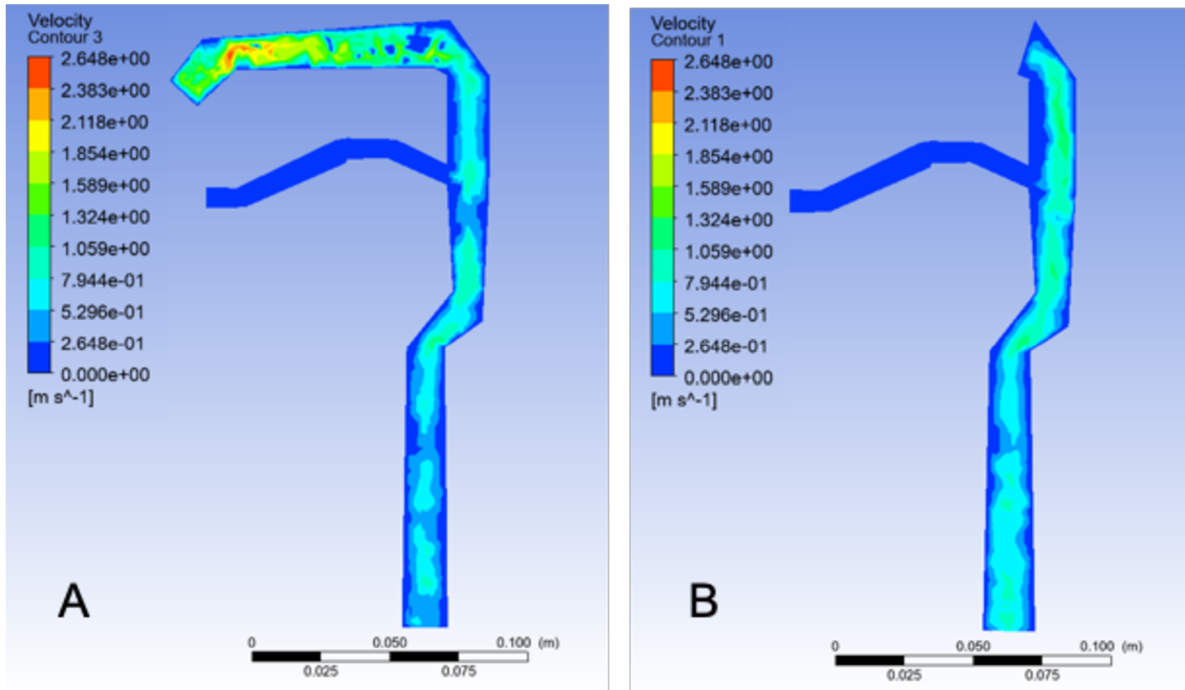


Figure 38: Velocity of the air flow inhaled through the nose, A: Cross section of the plane of the left nasal cavity, B: Cross section through the median plane

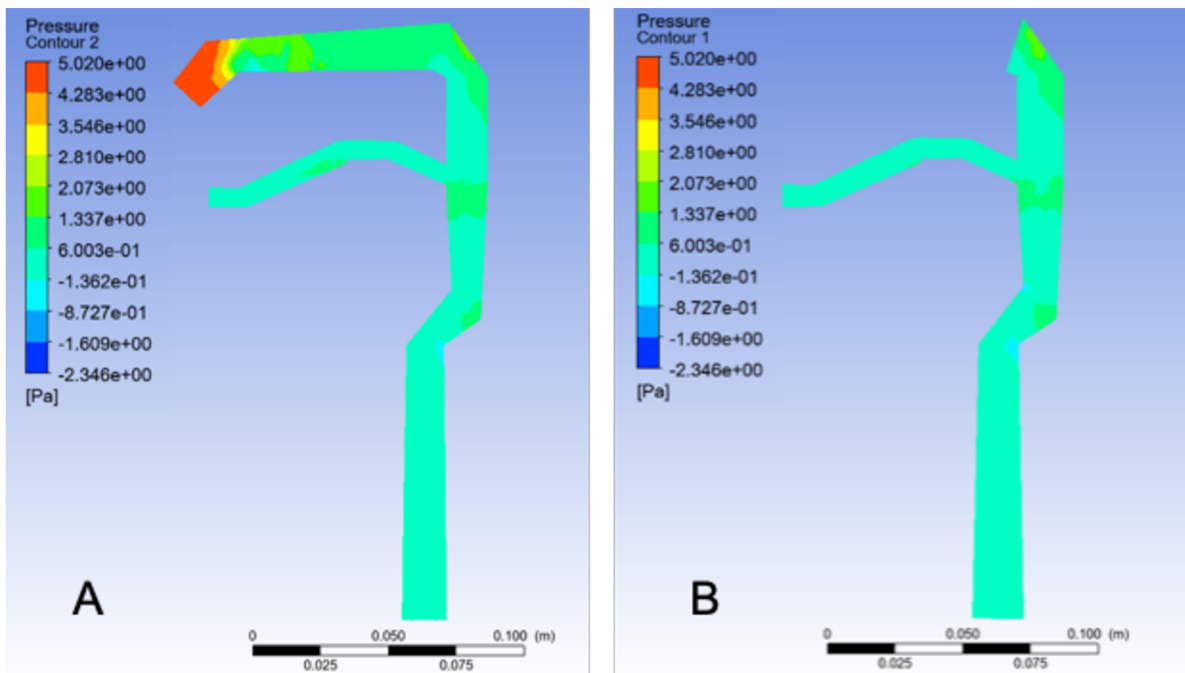


Figure 39: Pressure of the air flow inhaled through the nose, A: Cross section of the plane of the left nasal cavity, B: Cross section through the median plane

Characteristics of air flow inhaled through the mouth and nose with first sampling gap

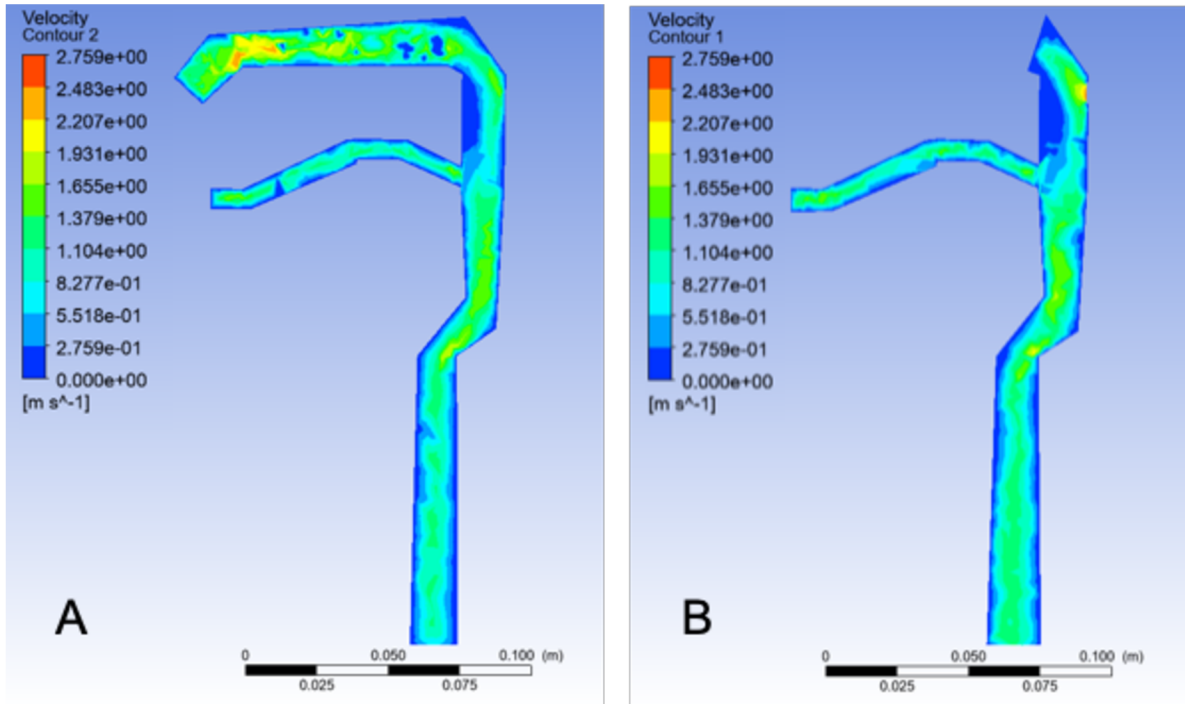


Figure 40: Velocity of the air flow inhaled through the mouth and nose with first sampling gap, A: Cross section of the plane of the left nasal cavity, B: Cross section through the median plane

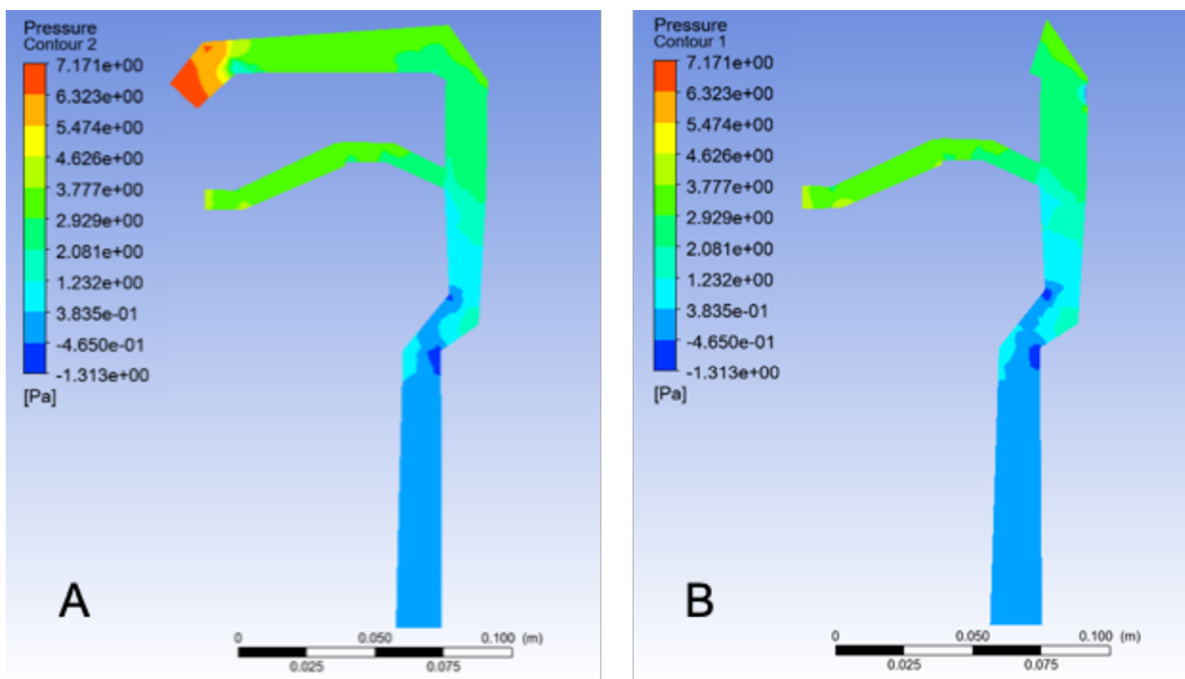


Figure 41: Pressure of the air flow inhaled through the mouth and nose with the first sampling gap, A: Cross section of the plane of the left nasal cavity, B: Cross section through the median plane

Characteristics of air flow inhaled through the mouth and nose with second sampling gap

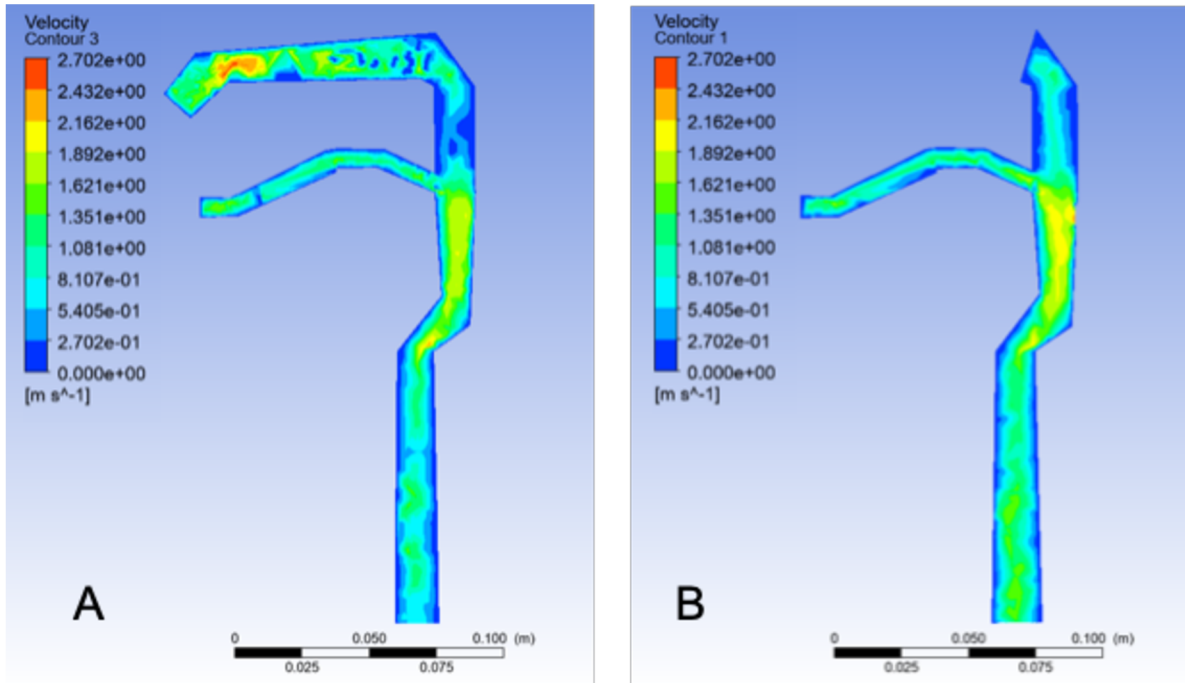


Figure 42: Velocity of the air flow inhaled through the mouth and nose with the second sampling gap, A: Cross section of the plane of the left nasal cavity, B: Cross section through the median plane

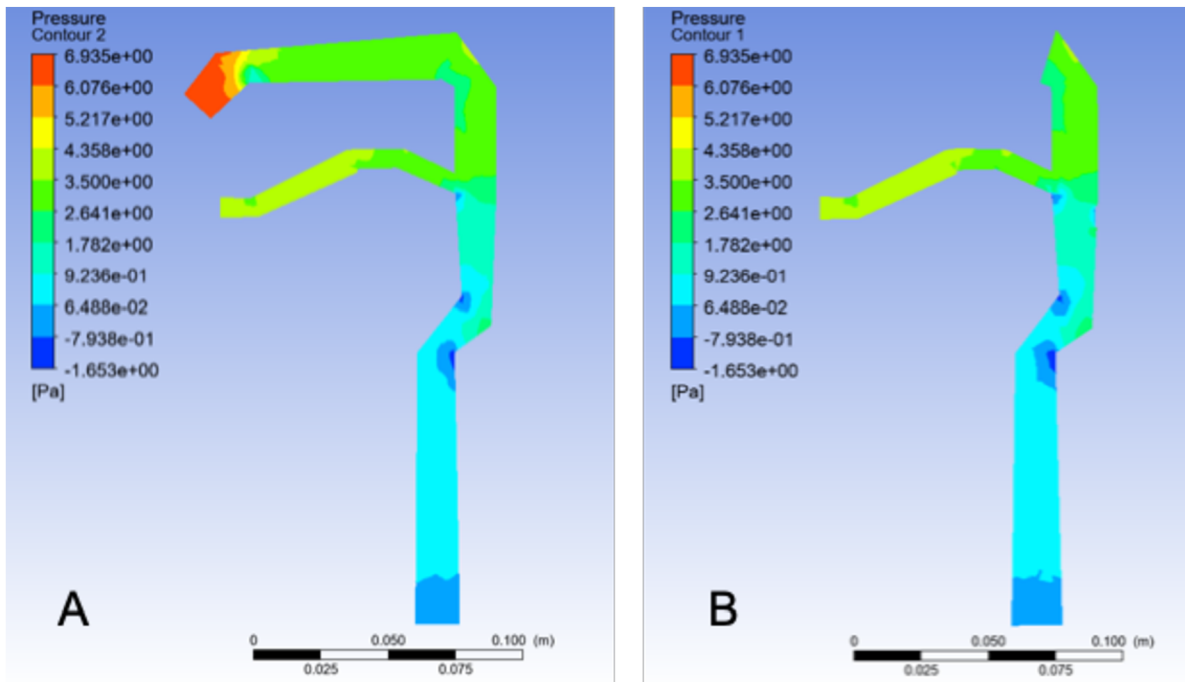


Figure 43: Pressure of the air flow inhaled through the mouth and nose with the second sampling gap, A: Cross section of the plane of the left nasal cavity, B: Cross section through the median plane

Characteristics of air flow inhaled through the nose with the first sampling gap

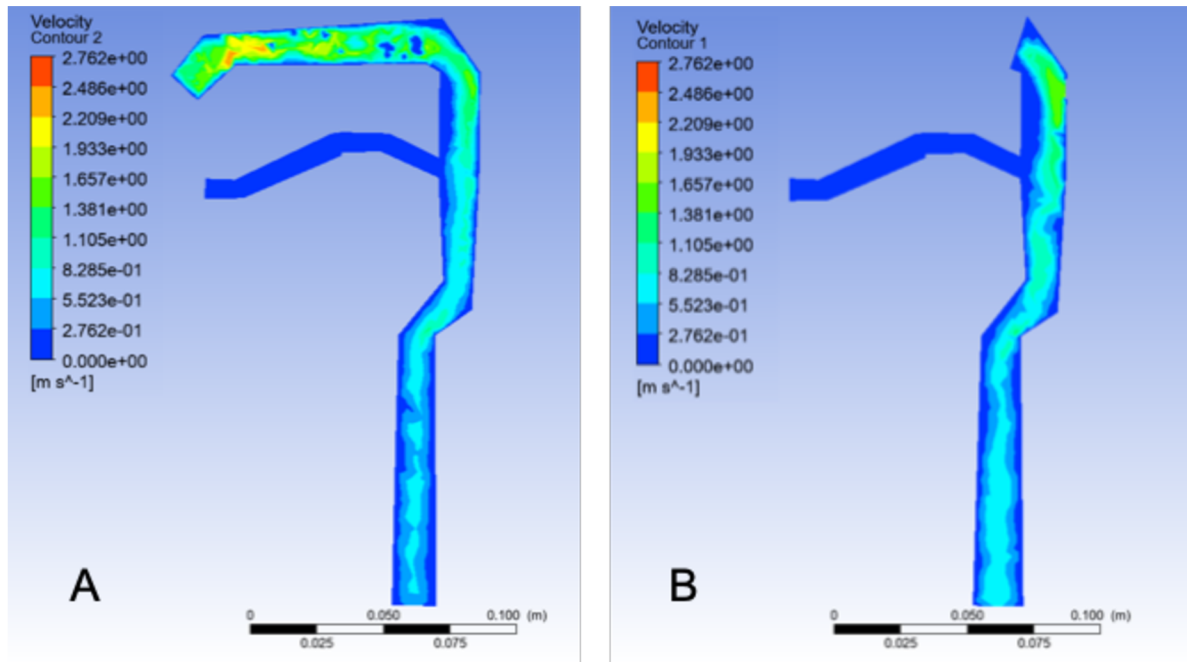


Figure 44: Velocity of the air flow inhaled through the nose with the first sampling gap, A: Cross section of the plane of the left nasal cavity, B: Cross section through the median plane

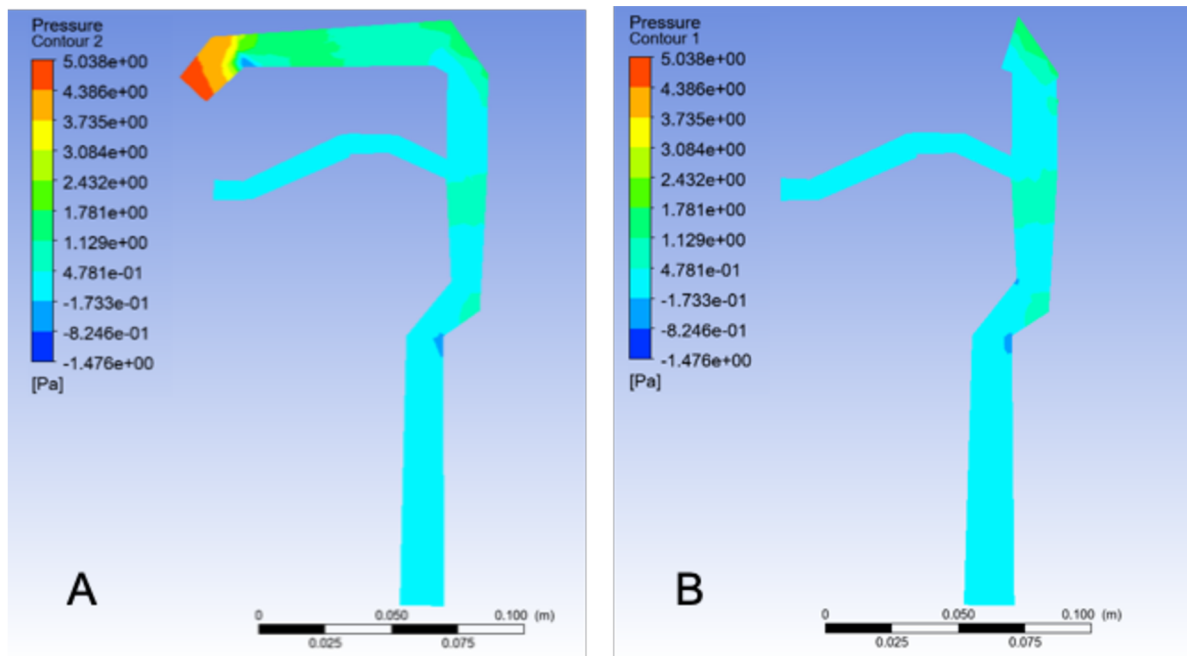


Figure 45: Pressure of the air flow inhaled through the nose with the first sampling gap, A: Cross section of the plane of the left nasal cavity, B: Cross section through the median plane